Adve

Advanced Functional Materials / Volume 31, Issue 49 / 2107363

Review | Full Access

Recent Progress on Metal-Based Nanomaterials: Fabrications, Optical Properties, and Applications in Ultrafast Photonics

Bo Fu, Jingxuan Sun, Yuan Cheng, Hao Ouyang, Giuseppe Compagnini, Peng Yin, Songrui Wei, Shaojuan Li, Dabing Li, Vittorio Scardaci, Han Zhang

First published: 20 September 2021
https://doi.org/10.1002/adfm.202107363
Citations: 1

Abstract

Nanomaterials have demonstrated excellent mechanical, thermal, optical, and electrical properties in various fields, including 1D carbon nanotubes, as well as 2D materials starting from graphene. Metal-based nanomaterials, mainly divided into metal and metal oxide nanoparticles, also gradually come into the sight of ultrafast photonics applications due to the outstanding optical properties. The optical properties of metal nanoparticles can be enhanced by the interaction between conduction electrons with electric fields that is called surface plasmon resonance. As for metal oxide nanoparticles, optical properties are closely related to bandgap structures. When it comes to transition metal oxides, other phenomena also play important roles in optical absorption such as spin inversion and excitons of iron. Moreover, preparation methods of materials are also crucial for their properties and further applications. Therefore, in this review, commonly used physical and chemical fabrication methods for metal-based nanomaterials are first introduced. Then the optical properties of typical metal and metal oxide nanoparticles are discussed specifically. In addition, the applications of metal-based nanomaterials in ultrafast lasers based on mode-locked and Q-switched techniques are also summarized. Finally, a summary and outlook toward the synthesis, optical properties, and applications in ultrafast photonics of metal-based nanomaterials are presented.

1 Introduction

Loading [MathJax]/jax/output/HTML-CSS/fonts/STIX-Web/Normal/Italic/Main.js

Metal-based nanomaterials have attracted wide research interest due to the excellent chemical and optical properties that often combine together, making them attractive in various fields such as photonics, sensing, catalysis, and biology.[1-5] Metal-based nanomaterials can be divided into two main sub-categories of pure metal nanoparticles (MNPs) and metal oxide nanoparticles (MONPs). Noble MNPs are also known as plasmonic NPs, because their optical properties are dictated by a unique interaction of conduction electrons with electric fields, which is known as surface plasmon resonance (SPR).[6] The SPR is related to the size and shape of NPs and influenced by the surrounding environment.[6] Moreover, the optical properties of MONPs are strongly related to their bandgap, and additional optical features may also arise for some transition metals owing to spin inversion or interaction with the oxygen atoms in crystal lattice.[7, 8] In order to cope with the expanding range of applications, a variety of chemical or physical methods have been proposed over the years for the production of MNPs and MONPs, which was also beneficial to ultrafast photonics applications including the development of ultrafast lasers.

Ultrafast lasers can generate ultrashort pulses with short pulse width and high peak power, which make them attract attention in various fields.[9-14] Equivalent saturable absorption devices such as nonlinear polarization rotation, nonlinear optical loop mirrors, and nonlinear amplifying loop mirrors are traditional methods to achieve ultrafast operation.[15-17] But the environmental instability or the need for precise control of power splitting hinder their applications. The emergence of semiconductor saturable absorber mirror provides a kind of real saturable absorber (SA) for the generation of ultrashort pulses, whereas the narrow bandwidth is still a limitation.[18, 19] Thereafter, nanomaterials as SAs come into the sight of researchers since the first demonstration of 1D carbon nanotubes in ultrafast lasers.[20-25] Subsequently, 2D materials including graphene,[26-32] topological insulators (TIs),[33-38] transition metal dichalcogenides (TMDs),[39-45] black phosphorus (BP),[23, 46-51] and MXenes[52-57] have also been widely used.[58-64] It is noted that 2D materials have several similar properties of broadband nonlinear response, high conductivity, and tunable bandgap that are required for SAs.[65-72] Graphene is consisted of single-layer carbon atoms in a honeycomb structure.[73] It has excellent advantages of ultrafast recovery time and broadband operation benefit from zero bandgap, but the modulation depth of 2.3% per layer is a limitation for wider applications.[26, 32] TIs are a kind of material with insulating bulk state and Dirac structure.[74] TIs have band structure similar to graphene that make them also have broadband nonlinear responses.[75] However, the fabrication process is still complex in use. TMDs possess a typical formula of MX_2, in which M is transition metal and X is chalcogen.[76] Although the bandgap of TMDs is tunable and depends on the number of layers, the large bandgap is not beneficial to generate ultrafast pulse in mid-infrared band.[77] BP is composed of only one element and the forces between individual layers are van der Waals forces.[78] Lasers based on BP-SA in 3.5 μm have been

Loading [MathJax]/jax/output/HTML-CSS/fonts/STIX-Web/Normal/Italic/Main.js

he development.[79] As a kind of

transition metal carbides, nitrides or carbonitrides, MXenes exhibit excellent properties of high electrical conductivity, high optical transparency, and large nonlinear coefficient.[53] Whereas acid etching is the typical method to fabricate MXenes, it is worth for us to explore more etchant with lower material damage and safer than acid solution.[80] Therefore, researchers will not stop searching for other materials with superior properties to meet diverse needs of lasers. Recent studies have exhibited that both MNPs and MONPs show strong optical nonlinearities with a fast recovery time, which make them attractive for the realization of a series of photonic devices, including pulsed lasers based on Q-switched and mode-locked techniques.[81-87]

In this review, we introduce the synthesis methods that have been used to produce metal-based nanomaterials. Then the optical properties of MNPs and MONPs, such as plasmonic and nonlinear optical properties are described, respectively. Considering the applications in ultrafast photonics, we discuss the typical mode-locked and Q-switched results of such materials in various lasers. Finally, our perspectives and conclusions on the topic are also presented.

2 Synthesis Methods

Metal-based nanomaterials with excellent optical properties have various applications in ultrafast photonics, which can be fabricated by chemical and physical methods (**Figure** 1). Synthesis for fabricating metal-based nanomaterials fall into two main categories of chemical and physical methods. Chemical methods are bottom-up processes that produce nanoparticles with the use of chemistry starting from different metal compounds. Physical methods, on the other hand, are top-down processes that produce nanoparticles starting from same metal or metal compound in a different aggregation state. In this section, we aim to provide a brief overview of the most common methods in each category that have been used as an initial step toward the fabrication of an SA. **Table** 1 summarizes the materials used and the synthesis methods outlined in this section, along with their optical and saturable absorption properties.

Table 1. Metal-based nanomaterials used for ultrafast lasers

Material *a)*	Synthesis	Absorption *b)*	Laser [μm]	Modulation depth	Saturation intensity/fluence	Ref.
GNPs	Chemical synthesis	500–1500 nm	1.56	10.7%	6.91 MW/cm^2	[81]
GNPs	Ion sputtering	Broadband across NIR	2.78	–	–	[88]

Loading [MathJax]/jax/output/HTML-CSS/fonts/STIX-Web/Normal/Italic/Main.js

Material [a]	Synthesis	Absorption [b]	Laser [μm]	Modulation depth	Saturation intensity/fluence	Ref.
	evaporation	across NIR				
GNPs	Au ion reduction	520 nm	635 nm	–	–	[90]
GNRs	Seed-mediated growth	Broadband across NIR	1.56	18–23%	40-47 MW/cm^2	[91]
GNRs	Seed-mediated growth	900–1600	1.56	16%	19 MW/cm^2	[92]
GNRs	Seed-mediated growth	Broadband across NIR	1.56	4.10%	35.5 MW/cm^2	[93]
GNRs	Seed-mediated	1400–1600 nm	1.56	0.60%	266 MW/cm^2	[94]

a) Materials: gold nanoparticles (GNPs), nanorods (NRs), nanowires (NWs), nanobipyramids (NBPs), silver NPs (SNPs), nanoplates (NPTs), copper (Cu), ferroferric oxide nanoparticles (FONPs), ferric oxide (Fe_2O_3), zinc (Zn), nickel (Ni), titanium (Ti), vanadium (V), Indium (I), tin (T)

b) Absorption: Near-infrared region (NIR).

Loading [MathJax]/jax/output/HTML-CSS/fonts/STIX-Web/Normal/Italic/Main.js

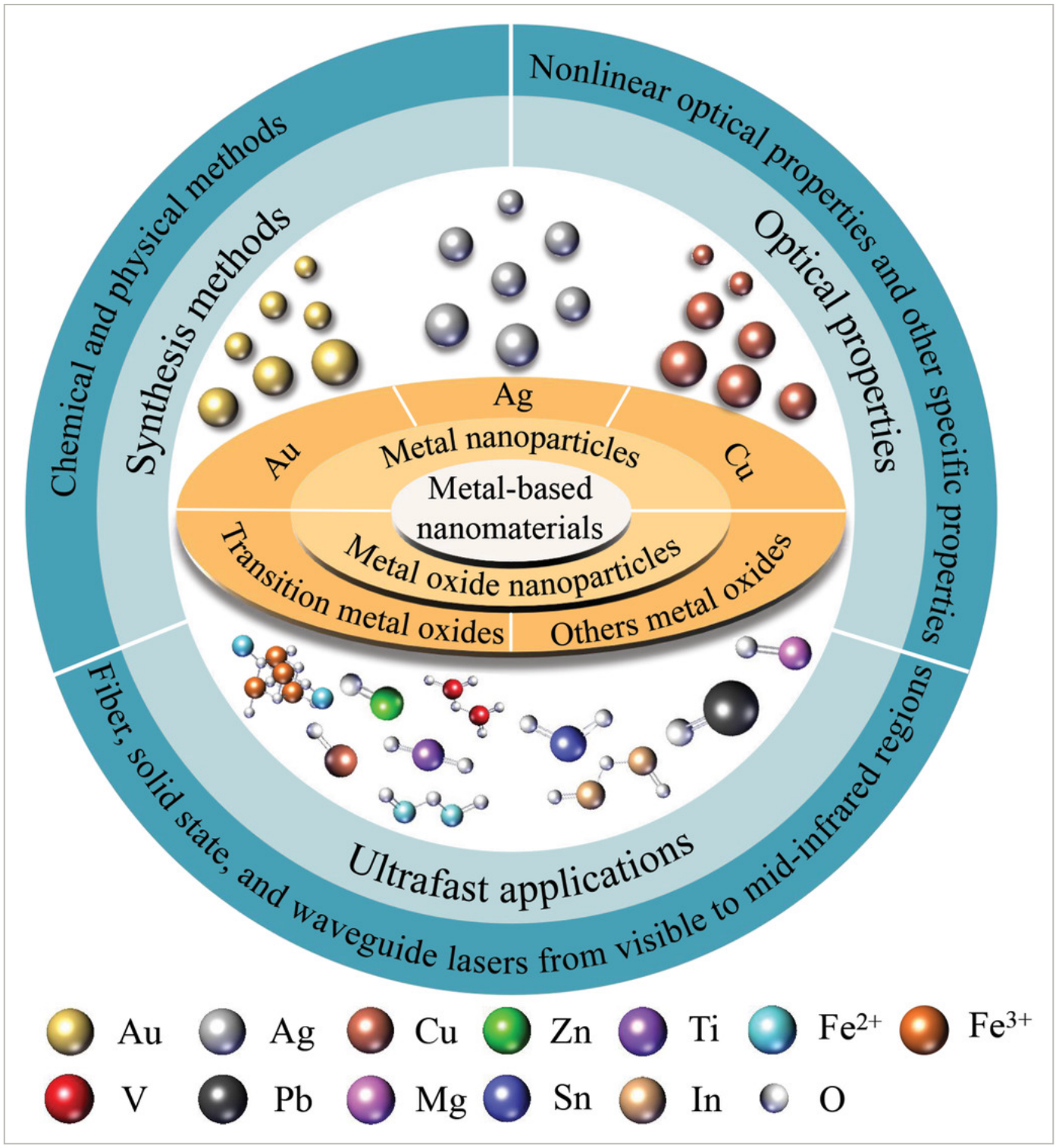

Figure 1

Open in figure viewer | PowerPoint

Synthesis, optical properties, and ultrafast applications of metal-based nanomaterials.

2.1 Chemical Methods

Loading [MathJax]/jax/output/HTML-CSS/fonts/STIX-Web/Normal/Italic/Main.js

Chemical reactions can be performed to obtain most pure metal and metal oxide-based nanoparticles that can then be utilized as SAs. The most popular pure metal NPs are gold (Au) and silver (Ag), and their syntheses are typically a salt of the metal ion reacting with a reducing agent under controlled reaction conditions.

For the chemical synthesis of spherical Au NPs (GNPs), an Au containing salt, chloroauric acid ($HAuCl_4$), is reduced by citrate in an aqueous environment under microwave heating. GNPs with an absorption band at 520 nm and an average diameter around 15 nm were produced and then used for the Q-switching of a 635-nm laser.[90] Non-spherical GNPs, around 20 nm in size, were prepared by a similar process and showed an absorption peak at 530 nm in solution. After being embedded in a carboxymethylcellulose (CMC) matrix, such GNPs showed a broadband absorption due to aggregation that extended into the near-infrared region (NIR). Such GNP-CMC composite can be used for a Q-switched laser at 1560 nm.[81]

Besides spherical NPs, a variety of different shapes can be made from Au to generate pulses in fiber lasers. Seed-mediated growth is a common approach to synthesize metal NPs of different shapes, which consists of two steps. An initial one where spherical nanoparticles or seeds are produced and the second one in which the seeds are transformed into different shapes.[126] For the production of Au seeds, $HAuCl_4$ is treated with cetyl trimethylammonium bromide (CTAB) and sodium borohydride ($NaBH_4$) and let it incubate for 2 h. After that, Au nanorods (GNRs) are obtained by adding the seed solution to a growth solution containing CTAB, bromosalicylic acid, silver nitrate ($AgNO_3$), and ascorbic acid.[127, 128] Through tuning the composition of the growth solution, it is possible to tune the aspect ratio of the NRs, and consequently adjust their absorption band across the NIR. Indeed, Shu et al. produced NRs with an average diameter of 58.7 nm and absorption band between 1400 and 1600 nm by typical seed-mediated growth (**Figure** 2), then utilized them for a 1560-nm soliton mode-locked laser.[94] GNRs produced by Kang et al. and Jiang et al. were also used for Q-switched lasers centered at 1560 nm, but they only exploited a tail of a broad absorption band between 900 and 1600 nm.[91, 92] In a separate experiment, Kang et al. fabricated a set of GNRs with an absorption band of 1000–2000 nm, then a mode-locked laser in 2 µm was achieved.[93] NRs with very high aspect ratio can be synthesized using a variation of the above method, which requires the use of nitric acid in a three-step process. Here, the formed seeds are first treated with $NaBH_4$ and then mixed to a growth solution containing CTAB, $HAuCl_4$, nitric acid, and ascorbic acid.[129] Wang et al. synthesized NRs with an aspect ratio mostly higher than 10 by this method, and generated mode-locked pulses at 1550–1560 nm.[95, 130]

Loading [MathJax]/jax/output/HTML-CSS/fonts/STIX-Web/Normal/Italic/Main.js

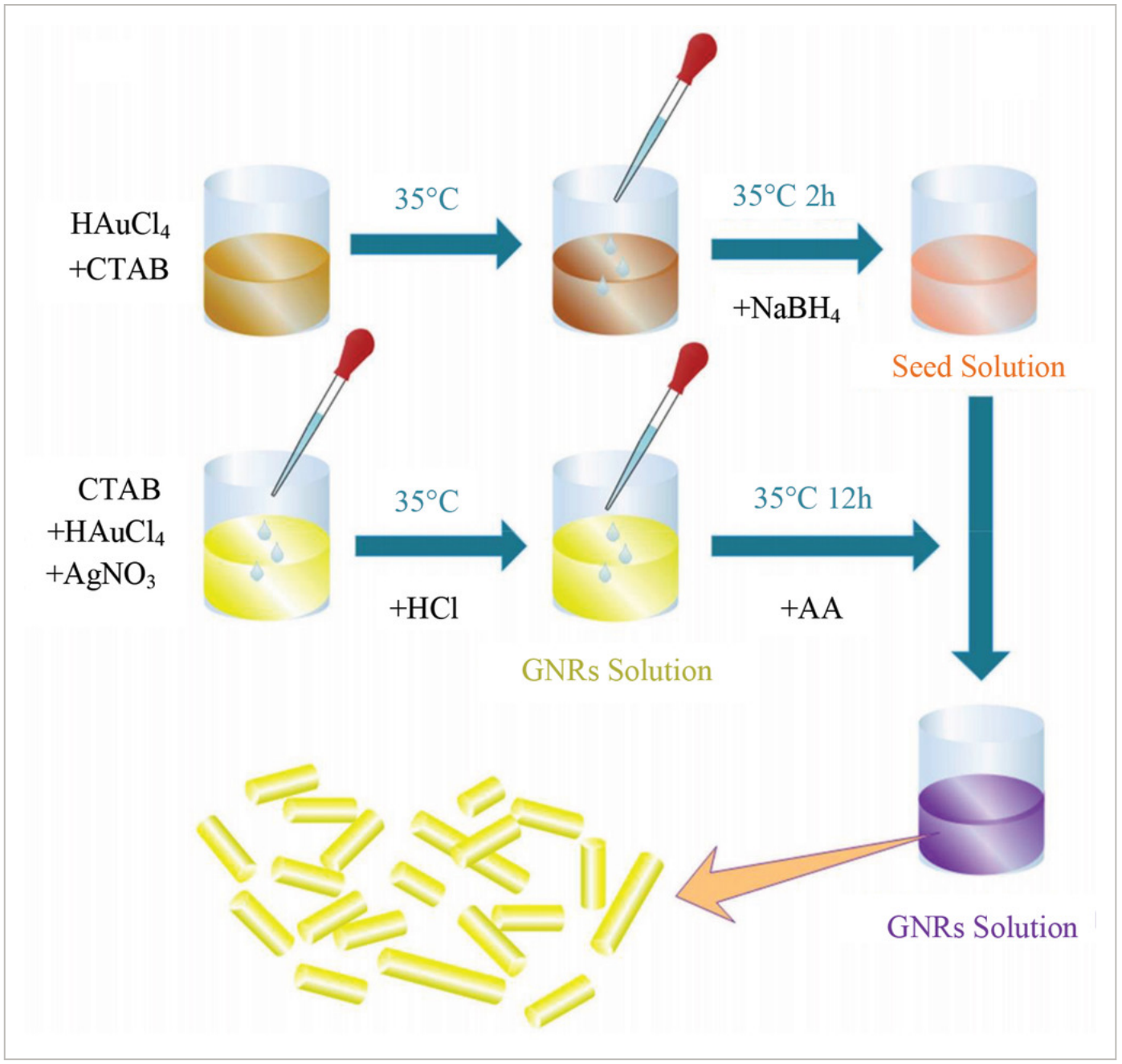

Figure 2

Open in figure viewer | PowerPoint

Schematic of a seed-mediated growth for GNRs. Reproduced under terms of the CC-BY license.[94] Copyright 2019, The Authors, published by Frontiers Media S.A.

A different type of Au nanostructure that was proposed as SA is gold nanobipyramids (G-NBPs), also obtained by seed-mediated growth. Here, Au seeds were prepared by adding $NaBH_4$ to a solution containing $HAuCl_4$, CTAB, and citrate. The seed solution was then added to a growth solution containing $AgNO_3$, ascorbic acid, and CTAB. The structures obtained by this method

Loading [MathJax]/jax/output/HTML-CSS/fonts/STIX-Web/Normal/Italic/Main.js

ell as an absorption peak around

1000–1100 nm, which were used for generating Q-switched pulses in a 1020-nm laser.[96] A similar process was also carried out by Zhang et al. to obtain G-NBPs with optical absorption around 1100 nm and Q-switched laser operation at 1061 nm.[97]

The seed-mediated growth method can also be applied for silver, as schematized in **Figure 3**. The process for obtaining shaped Ag NPs (SNPs) starts with the reduction of Ag^+ ions (typically from $AgNO_3$) by $NaBH_4$ in an aqueous environment to produce Ag seeds, where citrate ions are also present. Flat triangular nanoplates (NPT) are obtained when an $AgNO_3$ solution is added to a solution containing the seeds, hydrazine, and further citrate.[131] Seeds concentration as well as their addition rate regulate the final size of the NPTs, ranging from 50 to 200 nm, and thus the optical absorption spanning from 500 to 1100 nm. Indeed, higher seeds concentration yields smaller NPTs with limited red shift in visible region, while lower seeds concentration yields bigger NPTs with optical absorption red-shifted into NIR. This is because fewer seeds, in the same reaction conditions, are allowed to grow larger, while more seeds can only grow to some extent. Moreover, a faster seed addition rate limits the growth of the NPTs while a slower rate promotes the growth of larger NPTs. This is due to a competition between growth and secondary nucleation events. If the addition rate is slow enough, the former is favored and the NPTs grow larger, while if the addition is too fast the latter occurs limiting the growth.[131] Such NPT structures, with a broad absorption band from 900 to above 1300 nm, have been used in Q-switched and mode-locked lasers operating in 1 μm.[100, 101]

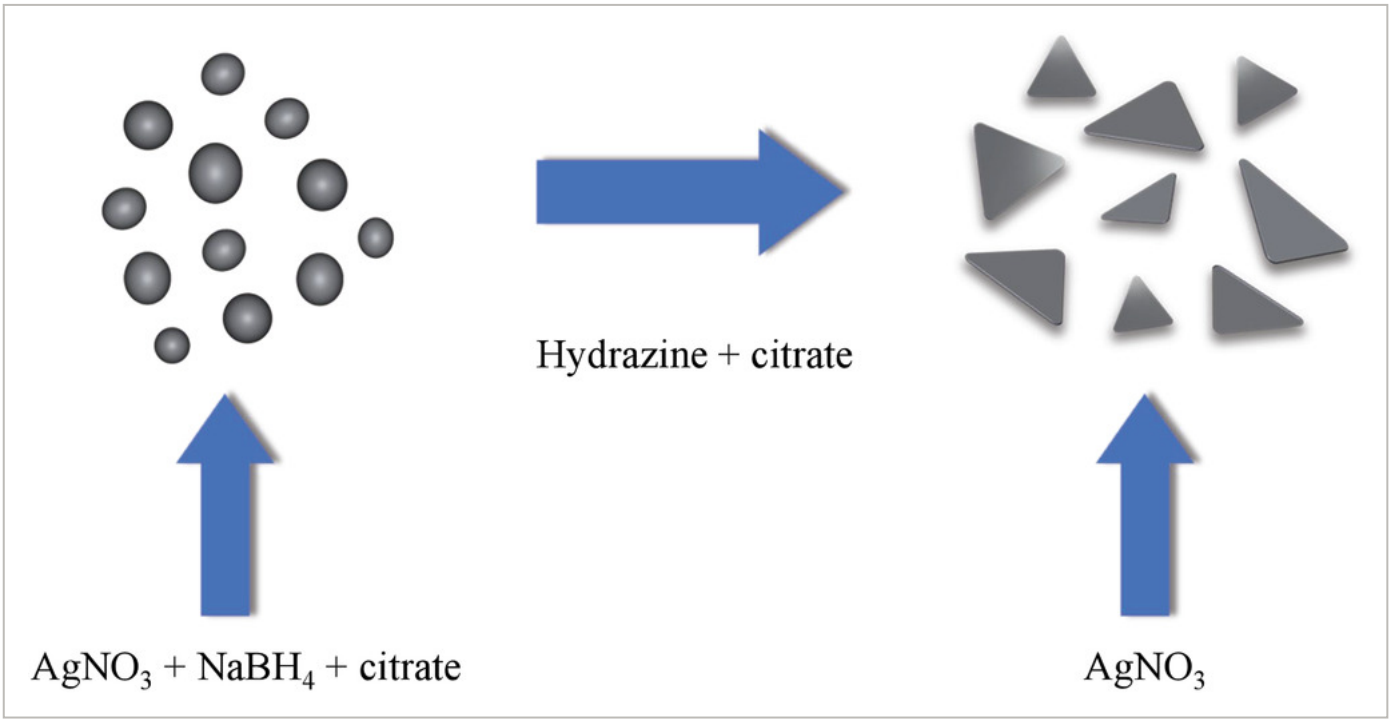

Figure 3

Loading [MathJax]/jax/output/HTML-CSS/fonts/STIX-Web/Normal/Italic/Main.js

Open in figure viewer | PowerPoint

Schematic of a seed-mediated growth for SNPTs.

Shaped metal-based nanoparticles can also be made using hydrothermal or solvothermal methods. A solvothermal method was used by Guo et al. to obtain Ag NPTs (SNPTs). Here, an $AgNO_3$ solution was added to a polyvinyl pyrrolidone alcoholic solution and heated to 180 °C in a sealed reactor. The process produced particles with mixed shapes and sizes ranging from 70 to 94 nm, which can be used to form Q-switched pulses at 1560 nm.[82]

A chemical method was used to produce copper nanowires (CuNWs). An aqueous solution containing cupric chloride and glucose is mixed with an ethanol solution containing oleylamine and oleic acid. After stirring at 50 °C for 12 h, CuNWs are obtained, and purified afterward by a series of centrifugation-redispersion-ultrasonication cycles.[132]

Among the metal oxides proposed for application as SAs, iron oxide is one of the most popular materials. Ferroferric oxide (Fe_3O_4) is commonly produced by a coprecipitation method, in which ferrous chloride and ferric chloride are used in an aqueous environment under nitrogen as external atmosphere and treated at 60 °C with ammonia. After a further ultrasound and stir process, Fe_3O_4 NPs (FONPs) are obtained, and further purified from chloride ions using water and ethanol.[107] Such process yields spherical NPs with an average diameter of 10–20 nm. If ferric oxide (Fe_2O_3) NPs are to be prepared, a similar process is used as first step to produce FONPs, where NaOH is employed instead of ammonia. After that, particles are oxidized to Fe_2O_3 by nitric acid at 90 °C. Such process yields spherical particles in size of 12–20 nm, which were then used with polyvinyl alcohol (PVA) composites in Q-switched fiber laser at 1-, 1.55-, and 2-µm wavelengths.[110] A thermal decomposition method was also proposed for the synthesis of FONPs for application as SAs. Here, $FeCl_3$ is dissolved along with sodium oleate in a solvent mixture made of water, ethanol, and hexane to obtain an iron-oleate complex after heating at 70 °C for 4 h. Such complex and oleic acid are dissolved in 1-octadecene and heated under stirring up to 320 °C for 1 h under nitrogen flow. After purification by centrifugation and washing, FONPs with an average size of 20 nm were obtained and used in a mode-locked fiber laser at 1558 nm.[108]

In order to obtain nickel oxide (NiO) NPs, also used as SAs, nickel chloride is treated with NaOH and subjected to ultrasonication. After the product of such reaction was separated by centrifugation, it is exposed to calcination at 350 °C to obtain the final NPs.[113]

Another metal oxide used as SA is zinc oxide (ZnO), in which most researches here used commercially available ZnO NPs. The exhaustive general information about the synthesis of ZnO NPs has also been summarized.[133-136] ZnO NPs have been used in one instance where they were synthesized by a hydrothermal method starting from zinc acetate dihydrate as precursor. This is mixed with NaOH and ammonia, then heated up to 60 °C before adding

Loading [MathJax]/jax/output/HTML-CSS/fonts/STIX-Web/Normal/Italic/Main.js

further NaOH until pH = 11 is reached. Subsequently, the mixture is brought into a sealed reactor at 180 °C for 24 h, where NRs are obtained as a white precipitate after washing and drying.[111]

Titanium oxide (TiO_2) NPs are typically discovered in nature under five different mineral forms. The two most common are rutile and anatase, which can be easily found commercially and are the starting materials when preparing TiO_2 NP-based SAs. A chemical method to obtain TiO_2 NPs is alkaline fusion, where rutile is mixed with NaOH and calcinated at 550 °C for 3 h. After that, a sulfuric acid solution is added and stirred for 3 h at 80 °C before being finally washed and dried.[137] TiO_2 NPs fabricated by such process have been used for a Q-switched laser at 1560 nm.[117]

Other metal oxide materials that have found applications as SA can be obtained by chemical methods. Vanadium oxide (V_2O_5) can be synthesized starting from ammonium metavanadate, which is treated with a surfactant and subsequently with nitric acid. The precipitate is firstly dried at 90 °C and then calcinated at 500 °C, to obtain a powder showing particles of the order of several microns.[118-120] Indium tin oxide (ITO) nanocrystals can be chemically synthesized starting from the dissolution of metallic indium in sulfuric acid to obtain indium sulfate, followed by the addition of tin chloride by keeping the reaction under stirring at 70 °C and pH = 7 by NaOH. Particles in the region of 20–50 nm in size are obtained by subsequent washing, drying, and calcining.[121, 122]

2.2 Physical Methods

There are a few approaches where physical methods have been proposed to produce metal nanoparticles for SA fabrication. One of these is thermal evaporation, whereby Au is deposited onto a PVA film that was previously formed.[89] Here, a current of 10 kA passed through an Au coil under vacuum, allowing Au to evaporate and condense onto the PVA film. The same approach was used for depositing CuNPs.[104] For SNPs instead, an electron beam targeted Ag pellets inside a vacuum chamber until they were sufficiently heated to evaporate and deposited onto a PVA film, as shown in **Figure 4**.[99] In both cases, SAs presented a broadband absorption in NIR and were used at the telecom wavelength region around 1550 nm. Similarly, an electron beam method was used to deposit ITO films onto optical components for SA integration.[123]

Loading [MathJax]/jax/output/HTML-CSS/fonts/STIX-Web/Normal/Italic/Main.js

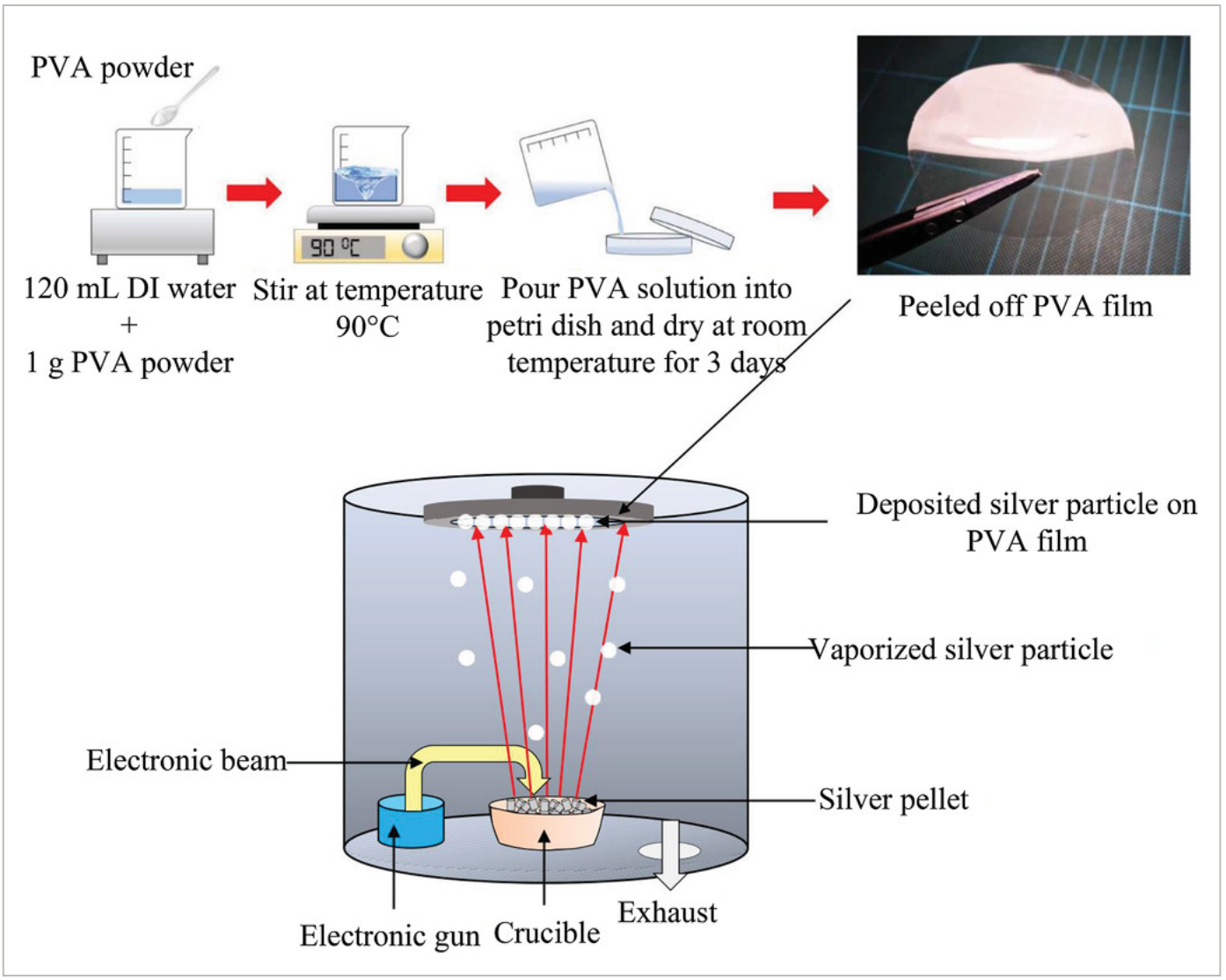

Figure 4

Open in figure viewer | PowerPoint

Schematic of SNPs deposition process involving an electron beam vaporizing Ag pellets, from which SNPs deposit onto a PVA film. Reproduced with permission.[99] Copyright 2019, Chinese Physical Society and IOP Publishing Ltd.

Ion sputtering is another approach that has been proposed for the fabrication of non-spherical GNPs used as SA, where the chamber was kept at 8-Pa pressure, the discharge current was 15 mA, and a discharge time of 20 s was used.[88] Particles with a size distribution centered around 100 nm were obtained and applied for Q-switching at 2780 nm.[88]

A physical method that was proposed to fabricate an Ag-based SA is ion implantation.[98] Ag ions were implanted into a neodymium-doped YAG crystal to fabricate a monolithic waveguide by using a 200-keV energy and a 5 × 10 16 -ions per cm^2 fluence at room temperature. Similarly, Cu ions were implanted into lithium niobate and lithium tantalate to obtain Cu NP-

Loading [MathJax]/jax/output/HTML-CSS/fonts/STIX-Web/Normal/Italic/Main.js

Physical methods are used for the preparation of TiO_2 NP from commercial rutile or anatase. For example, anatase can be dissolved in water with the aid of sodium dodecylsulphate followed by stirring and centrifugation. Then the supernatant was collected for integration within a PVA composite and used for a mode-locked laser near 2 μm.[116]

In summary, for MNPs the most utilized method is the seed-mediated growth, a chemical method that allows enough flexibility and control of the shape and size of NPs through the synthesis conditions. A mix of physical methods are also used, which seem to offer an easier production but with less control. For MONPs, a range of chemical methods are reported, each one specific for the type of material.

3 Optical Properties of Metal-Based Nanomaterials

For metal-based nanomaterials, optical properties are dependent on metallic or semiconducting/insulating characteristic of the related bulk material. For MNPs, these are strongly determined on the interaction of the surface conduction electrons with electromagnetic waves, generating the so-called SPR. On the other hand, the optical properties of MONPs are typically dictated by the optical bandgap. In both systems, nonlinear optical phenomena can be observed, especially saturable absorption.

3.1 Optical Properties of MNPs

The optical properties of metal nanoparticles are described by a phenomenon known as SPR, which represents a collective oscillation of surface electrons due to the interaction with an electromagnetic field. If the electric field oscillates with a wavelength significantly bigger than the NP, as electrons in a metal NP are free to move on its surface, a dipole is formed according to:

$$\mu = \alpha E \tag{1}$$

where μ is the dipole moment, α is the electric polarizability, and *E* is electric field. The polarizability α is related to the dielectric function according to:

$$\alpha = 4 \pi \varepsilon_0 R^3 \frac{\varepsilon - \varepsilon_m}{\varepsilon + 2\varepsilon_m} \tag{2}$$

where *R* is particle radius, ε is the dielectric constant of the metal, ε_0 is the dielectric constant in vacuum, and ε_m is the dielectric constant of the medium.[6] The maximum optical

Loading [MathJax]/jax/output/HTML-CSS/fonts/STIX-Web/Normal/Italic/Main.js

$\varepsilon = -2\varepsilon_m$. Hence for MNPs, the

optical properties depend on the type of metal (through ε), the particle size, and the surrounding medium (through ε m). Equation (2) is strictly valid only for spherical particles. Hence we expect dramatic changes as metal nanoparticles become anisotropic.[6, 138] As an example, **Figure** 5 shows the absorption spectra of Ag spherical NPs and flat NPTs. It can be observed that, while spherical NPs exhibit a single plasmon resonance, NPTs show four different features. This happens because now the particle has a size comparable to the wavelength of the electric field, and the electric field experienced is no longer constant across the particle, giving rise to dipole and quadrupole resonances both in-plane and out-of-plane. The in-plane dipole resonance is the main feature, significantly red-shifted from the plasmon resonance in the spherical NPs, depending on the size. The other important feature, though lower in intensity, is the out-of-plane quadrupole mode at 330–340 nm, which is a typical fingerprint of anisotropy in the structure.

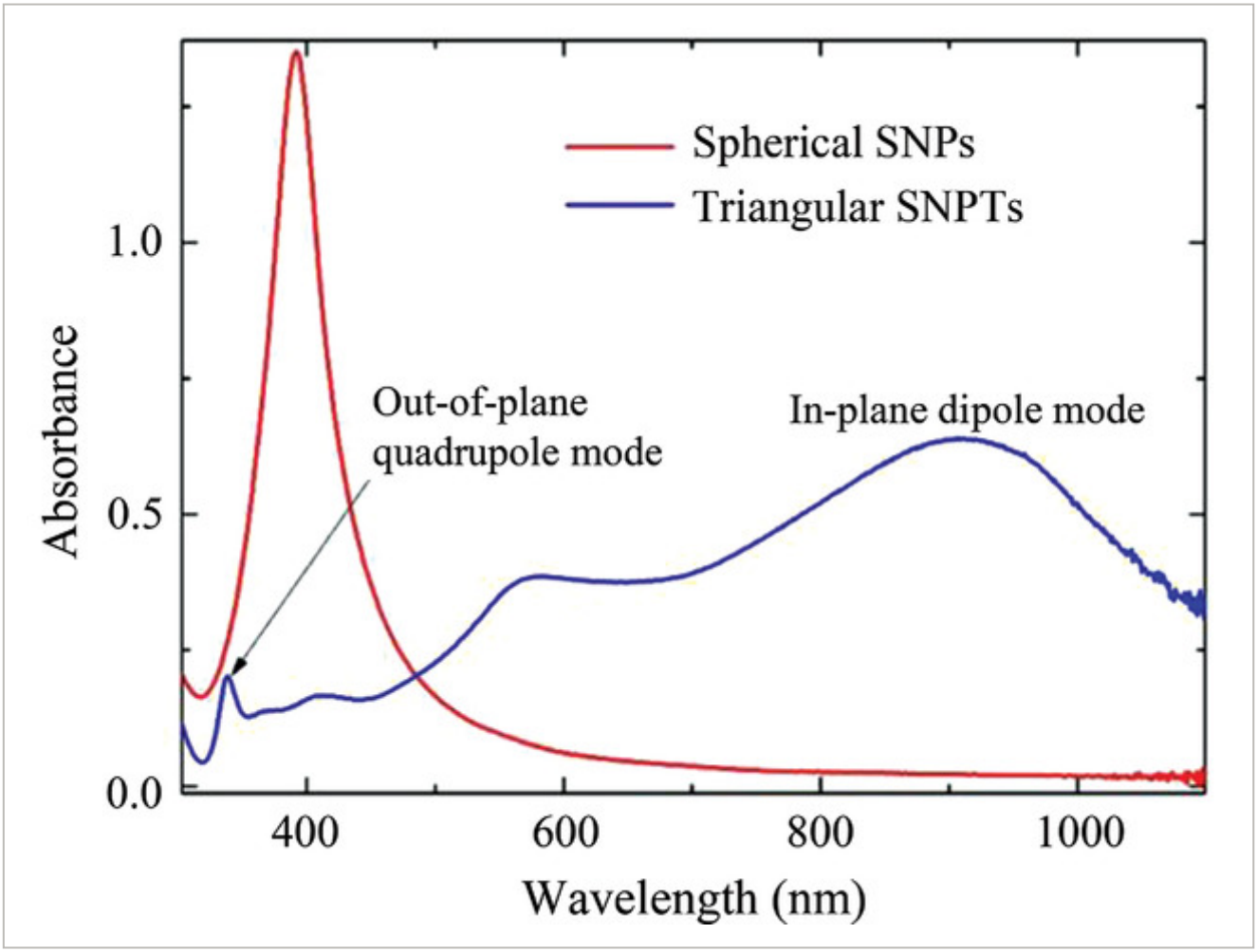

Figure 5

Open in figure viewer | PowerPoint

Absorption spectra of spherical SNPs and flat triangular SNPTs.

Loading [MathJax]/jax/output/HTML-CSS/fonts/STIX-Web/Normal/Italic/Main.js

3.2 Optical Properties of MONPs

Where the nature of nanoparticles is not metallic, their optical properties arise from different phenomena. Indeed, metal oxides can be semiconducting or insulating. In general, their optical properties arise from their band structure and are closely dictated by bandgap. Particularly, the optical absorption band is related to the bandgap of material, in which the peak wavelength increases with the decrease of bandgap, indicating that the material can operate in a broader band.[139-141] When transition metals are involved, the unique properties of the d-orbitals play a major role. The most popular MONPs used as SAs are Fe_2O_3 and Fe_3O_4. It is known that optical properties of Fe $3+$ come from three different phenomena. First, ligand field type transitions can be observed as the system is excited from the highest spin multiplicity, which is the ground state at lower energy, to a lower spin multiplicity. Second, the magnetic coupling of two adjacent Fe $3+$ ions can lead to the simultaneous excitation of both ions. Such process is known as pair excitation or double exciton process and lies at roughly double the energy of a ligand field transition. At a higher energy, we observe the ligand-to-metal charge-transfer transitions. The ligand in this case is the O $2-$ ion, which is responsible for the strong absorption below 400 nm with tails that extend well into visible region.[7, 8] Transitions related to the band edge also exist that overlap with the previously mentioned transitions and cause broadband absorption. For Fe_3O_4, the bandgap was estimated between 2 and 3 eV depending on morphology and particle size.[142-144] This translates into a strong optical absorption in the UV region that has a long tail up to 400–500 nm and may extend up to NIR.[143-146] For example, **Figure 6** shows an absorption spectrum of Fe_2O_3 nanocrystals in water.[144] Here, the feature at 450 nm is attributed to the ligand-metal charge transfer, while the band at 550 nm is attributed to pair excitons. Ligand field transitions are overlapped with charge transfer.

Loading [MathJax]/jax/output/HTML-CSS/fonts/STIX-Web/Normal/Italic/Main.js

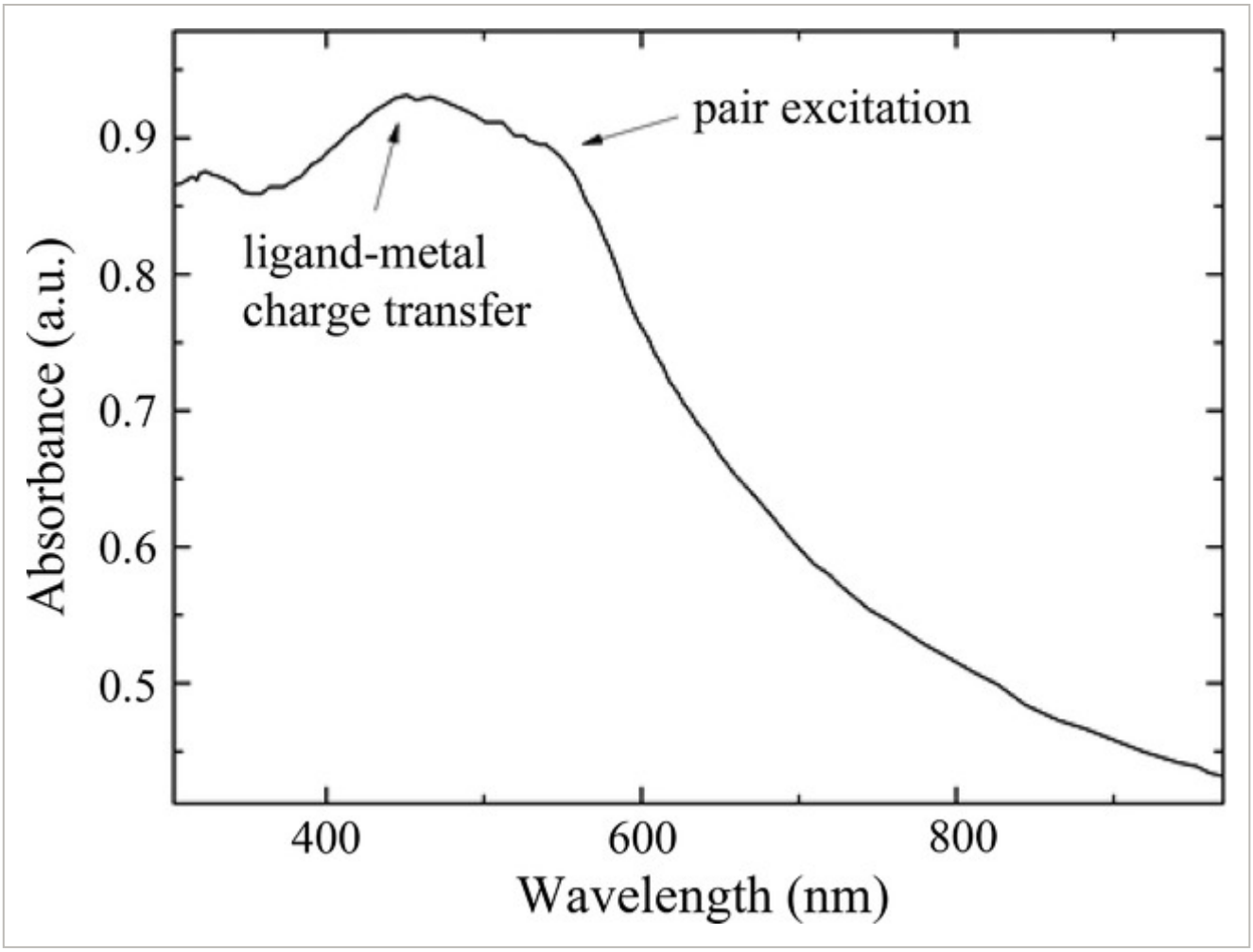

Figure 6

Open in figure viewer | PowerPoint

Optical absorption from Fe_2O_3 nanocrystals in water. Reproduced with permission.[144] Copyright 2009, American Chemical Society.

In NiO, CuO, and ZnO, the metal ions have their d-type orbitals partially or completely full, while in TiO_2 the Ti 4 + ions are deprived of electrons. For such reasons, unlike in iron oxide, these oxides cannot give optical transitions that are related to spin inversion or magnetic coupling, thus the optical properties in the UV–vis–NIR are strongly dependent on their bandgap.[147-150] In ZnO, the bandgap is 3.3 eV and causes a sharp transition around 370 nm, while in TiO_2 the bandgap is 3.2 eV and gives rise to a transition around 390 nm. SAs based on such oxides, which work in NIR, exploit their broadband absorption owing to the free carriers, yielding nonlinear optical effects.[151] In CuO, the bandgap is around 1–2 eV, energy transitions increase with the bandgap, which can be exploited by SAs.[152]

3.3 Nonlinear Optical Properties of Metal-Based Nanomaterials

Loading [MathJax]/jax/output/HTML-CSS/fonts/STIX-Web/Normal/Italic/Main.js

In linear optics, polarization *P* of a material is related to the electric field *E* as $P = \varepsilon_0 \chi^{(1)} E$, where ε_0 is the dielectric constant in vacuum and χ is the magnetic susceptibility. Under a very intense electric field, the response of the material becomes nonlinear, and the polarization is typically expressed as a power series expansion:[153]

$$P = \varepsilon 0 (\chi (1) E + \chi (2) E + \chi (3) E \dots) \quad (3)$$

Here, $\chi (1)$ is the linear susceptibility, while $\chi (2)$ and $\chi (3)$ are the 2 n d and 3 r d order nonlinear susceptibilities. Saturable absorption is one type of 3 r d order nonlinear susceptibility, which consists in increasing transmittance of a material under a very high intensity radiation. In short, the material becomes transparent under a very strong illumination. A simple way to describe the saturable absorption of a material is in terms of the absorption coefficient, which can be expressed as:

$$A = A 0 1 + I / I S + A N S \quad (4)$$

where A_0 is the linear limit of saturable absorption, *I* S is the saturation intensity, and *A* N S is the non-saturable absorption component. From the above equation, it can be clearly seen that the overall absorption *A* decreases with the increase of radiation intensity *I*. The saturation intensity *I* S is thus defined as the intensity needed to decrease A_0 to 50% of the initial value.[153] This is clearly a very important parameter for an SA as a low *I* s indicates that the system needs a low intensity to reach saturation, thus a low *I* S is desirable. A summary of the *I* S values reported for metal NPs can be found in Table 1.

From a practical standpoint, one important property of SAs is the modulation depth, defined as the maximum transmittance variation (ΔT) that a material can undergo with the increase of light intensity at a set condition. Modulation depth is commonly measured when nanomaterials are used as SAs. It is important to note that, while $\chi (3)$ is an intrinsic property of the material, the modulation depth and saturation intensity are more properties of the SA device than the material. Indeed, they will depend not just on the material but also on the processing and the integration method. A summary of the modulation depths measured from metal-based NPs is also presented in Table 1.

There are two main methods to measure saturable absorption of materials. In z-scan method, as schematized in **Figure** 7a, a pulsed laser is focused by a lens and a detector is placed along the beam propagation direction (the z-direction). The transmittance of material is measured as a sample moves across the direction. Since the beam intensity is the highest near the focus (normally indicated as z = 0), the sample material experiences the highest light intensity and

Loading [MathJax]/jax/output/HTML-CSS/fonts/STIX-Web/Normal/Italic/Main.js

optical nonlinearities can thus be observed. If an aperture is placed in front of the detector (closed aperture z-scan method) a nonlinear refractive index can be measured, as the sample material will act as a lens by self-focusing and self-defocusing the beam in the proximity of the z = 0 position. Since the aperture will let only a portion of the beam into the detector, when the material is self-focusing, the transmittance would increase, while as the material is self-defocusing the transmittance would decrease. In order to measure saturable absorption, a z-scan system has to operate in an open aperture configuration, that is, without any aperture in front of the detector which should be able to capture the entire beam. In this case, the transmittance will increase around the z = 0 position. On the other hand, if transmittance decreases, we rather observe optical limiting.[154] Sometimes saturable absorption is referred to as reversed optical limiting.

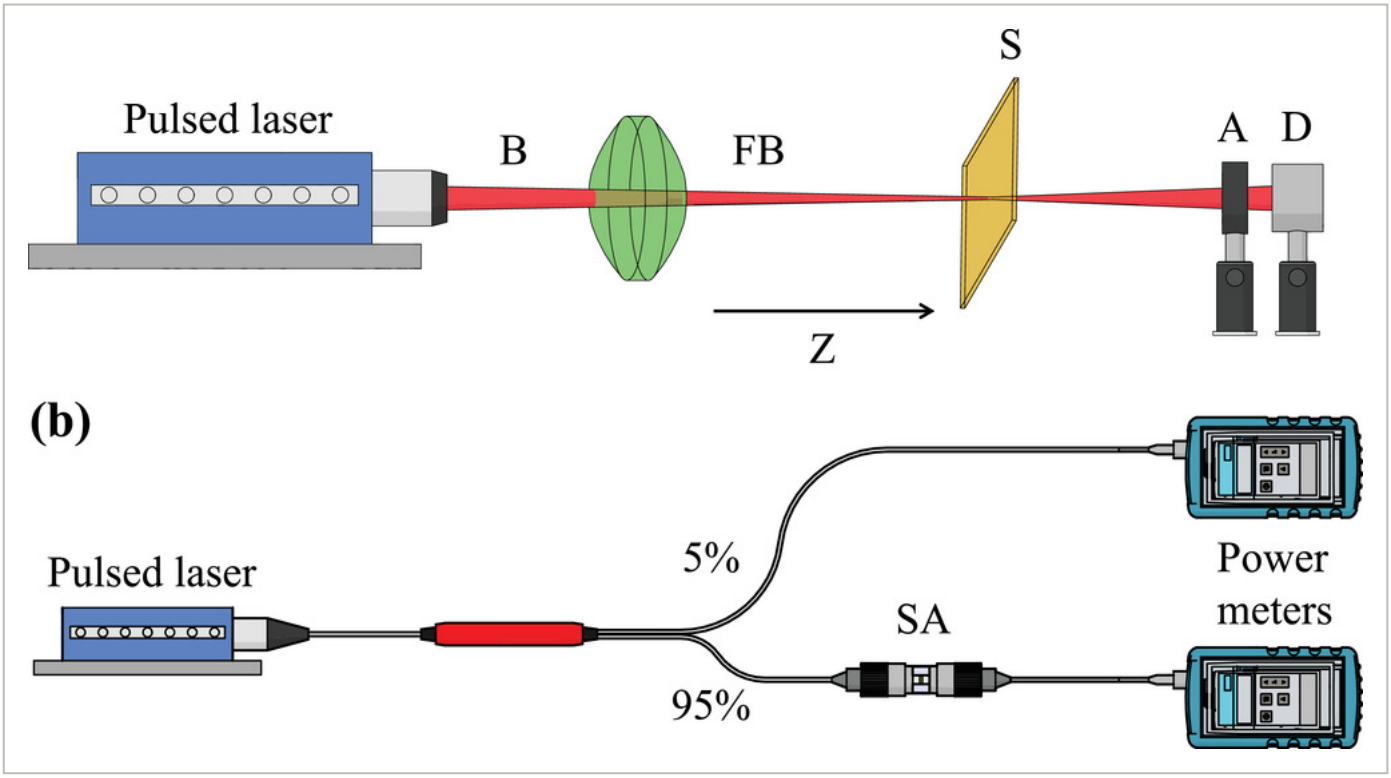

Figure 7

Open in figure viewer | PowerPoint

a) Schematic of a z-scan setup. B: laser beam; FB: focused laser beam; S: sample; A: aperture; D: detector. b) Schematic of a power dependent transmittance measurements setup.

The other method to measure saturable absorption is performing power dependent measurement, allowing a direct determination of the modulation depth. Usually, a pulsed laser source at the wavelength of interest is used. The laser beam is split into two paths, one of which is used as a reference while the other is for the actual transmittance measurement, as shown schematically in Figure 7b. By increasing the laser power, the transmittance increases

Loading [MathJax]/jax/output/HTML-CSS/fonts/STIX-Web/Normal/Italic/Main.js

while the sample is in the linear regime and shows a plateau as the sample reaches the saturation regime.

In summary, the optical properties of MNPs are deeply dependent on their size and shape through the strong interaction of their conduction electrons with electromagnetic fields. MONPs instead have optical properties deeply related to their optical bandgap. In some of the transition metals, like Fe, other phenomena also contribute to optical absorption, like spin inversion and excitons. In all cases, saturable absorption occurs, making these materials suitable candidates for the passive generation of laser pulses through the Q-switched or mode-locked mechanisms. While this is stronger in resonance with an absorption peak, given by SPR or bandgap for MNPs or MONPs, respectively, saturable absorption in NIR for MONPs is far from the bandgap and is typically due to the free carriers.

4 Applications of Metal-Based Nanomaterials in Ultrafast Lasers

In the process of generating ultrafast pulses using SAs, the choice of materials with excellent saturable absorption properties is a crucial part. As a kind of 1D saturable absorber (SA) material, carbon nanotubes have advantages of high modulation depth and damage threshold, but the insertion loss caused in specific region is a drawback that needs to be solved.[155] Afterward, since graphene was exploited to achieve ultrafast pulses in lasers, other typical 2D materials including graphene, TIs, TMDs, BP, and MXenes were also used to realize pulsed lasers. However, a few limitations still hinder their further applications. The modulation depth of graphene is only 2.3% per layer, which can seriously affect the performance as SAs.[26, 32] TIs have complex fabrication processes that also restrict the further application in various fields.[156, 157] The main drawback of TMDs is the large bandgap, making them difficult to generate ultrafast pulse in mid-infrared lasers.[77] With regard to BP, the easy oxidation in air has to be improved.[158] The family of MXenes consists of dozens of materials with distinct properties, but only part of them have been explored.[55] In recent years, MNPs have attracted wide attention in several fields due to their excellent electrical, magnetic, and chemical properties.[159-161] Furthermore, other properties have also been gradually investigated for applications in ultrafast photonics. On the one hand, MNPs have remarkable nonlinear optical properties, including large nonlinear absorption coefficient and fast recovery time, which are required for applications as saturable absorbers, proving the potential for generating ultrafast pulses.[162-164] On the other hand, MNPs have strong localized SPR caused by collective oscillations of conducting electrons, which is also beneficial to enhance the nonlinear absorption.[165-167] It is known that the SPR properties can be adjusted by changing the shape of nanoparticles, which is also of great significance to optimize the saturable absorption properties.[163, 168] Moreover, rbers due to their various

Loading [MathJax]/jax/output/HTML-CSS/fonts/STIX-Web/Normal/Italic/Main.js

outstanding optical properties, such as tunable bandgaps without changing physical properties, as well as good thermal and chemical stabilities.[169-171] Therefore, in order to better investigate the status of ultrafast applications of metal-based nanomaterials, we cover their typical results in lasers in two separate sections for MNPs (Section 4.1) and MONPs (Section 4.2).

4.1 Metal Nanoparticles

4.1.1 Gold

Au has high third-order nonlinear coefficient and excellent saturable absorption properties governed by the excitation of localized SPR, which make it a promising SA candidate for ultrafast lasers.[162, 172] In previous works, many researches focused on the theoretical studies of gold nanomaterials as SAs.[173, 174] In 2012, Jiang et al. reported the first demonstration of using non-spherical GNPs as SA to generate a passive Q-switched pulse in an Er-doped fiber laser (EDFL).[81] In this work, a GNP-CMC film exhibited broadband absorption that enabled a fiber laser to Q-switch at 1560 nm. Since then, ultrafast lasers enabled by gold nanomaterial-based SAs have been extensively investigated. In 2015, Wu et al. firstly used GNPs as SA to generate ultrafast pulse, in which a Q-switched pulse with a wide range of repetition rate from 285.7 to 546.4 kHz was realized in 635-nm visible region.[90] In 2017, Ahmad et al. reported on a 1.5-μm mode-locked pulsed laser enabled by a GNPs-SA, where the laser operated in S-band (1460–1530 nm) because of the gain of Tm-doped fluoride fiber in this region.[175] In 2018, Zhang et al. firstly proposed a non-spherical GNP-SA for realizing Q-switched pulses in Er:ZrF_4-BaF_2-LaF_3-AlF_3-NaF (ZBLAN) fiber laser at the wavelength of 2.78 μm, in which the average output power of 337 mW with the single pulse energy of 3.58 μJ was achieved.[88] In 2020, Rosol et al. obtained a stable mode-locked nanosecond pulse in a GNPs-based EDFL, where the PVA film was applied to integrate GNPs into laser cavity.[176]

GNRs have anisotropic SPR due to their non-spherical symmetric structure. Therefore, GNRs have transverse and longitudinal SPR absorption caused by electron resonance perpendicular to and along the rod axis, respectively, which can broaden the operating wavelength.[177-179] In 2013, Kang et al. used GNRs-NaCMC films as SAs in an EDFL and obtained mode-locked and Q-switched pulses operated in 1561 and 1560 nm, respectively, proving the ability of GNRs-based SAs to generate ultrafast pulses.[92, 180] In 2014, Wang et al. achieved a mode-locked pulse with duration of 887 fs at the wavelength of 1552 nm, in which the optical damage threshold of GNRs-SA could be enhanced by using microfiber-based GNRs.[95] **Figure** 8a shows the transmission electron microscopy (TEM) image of GNRs with a few nanoparticles. The optical spectrum, autocorrelation trace, and corresponding radio frequency (RF) spectrum of the mode-locked pulse are shown in Figure 8b–d, respectively. Then, Kang et al. implemented a pulsed laser in 1039 nm by GNRs-based SA for the first time, where a stable passively mode-locked [181] Subsequently, in 2015, they firstly obtained a mode-locked pulse in 1982 nm by inserting a GNRs-SA into Tm-doped fiber laser (TDFL) cavity.[93] These

Loading [MathJax]/jax/output/HTML-CSS/fonts/STIX-Web/Normal/Italic/Main.js

results indicated that GNRs are also excellent SA candidates for 1- and 2-μm lasers. In 2016, Wang et al. presented a wavelength-switchable femtosecond pulsed laser by properly adjusting the cavity parameters, in which the optical properties and thermal stability of GNRs-SA can be improved via coating the surface of GNRs with a silica shell (i.e., GNRs@SiO_2).[130] Besides, they also investigated other fiber lasers based on GNRs-SAs, which can provide flexible switchable pulse sources to satisfy different requirements in ultrafast applications.[182, 183] Furthermore, Lee et al. proposed an end-to-end self-assembly technique that can red-shift the wavelength absorption band of GNRs from 1.5 to 1.9 μm, and it has been proved in Er-doped and Tm-Ho co-doped fiber lasers.[184] In 2017, Lee et al. reported on an Yb-doped fiber laser (YDFL) enabled by a self-assembled GNRs-SA, in which a mode-locked soliton with a pulse duration of 840 fs was generated at the wavelength of 1063.9 nm.[185] Jiang et al. used GNRs-SA to construct a 1.5-μm Q-switched ultrafast laser, obtaining tunable pulse duration and repetition rate by introducing a modulation light.[91] In 2018, Lu et al. demonstrated a passively mode-locked fiber laser based on GNRs-SA at 1041 nm, where a stable dissipative soliton was achieved with a signal to noise ratio (SNR) greater than 70 dB.[186] Kang et al. obtained a stable 404-fs mode-locked pulse with a maximum average power of 45.5 mW in an all-fiber Tm-doped laser, which is mode-locked by a microfiber coated with GNRs.[187] In 2019, Shu et al. exploited GNRs as high-performance SA to generate a stable mode-locked pulse in an EDFL, and ninth-order harmonic mode-locked soliton molecules were also observed in the cavity for the first time.[94] In 2020, Cui et al. used a same SA based on GNRs/D-shaped fiber to achieve mode-locking in EDFL and TDFL, indicating its ability of broadband operation in ultrafast lasers.[188]

Loading [MathJax]/jax/output/HTML-CSS/fonts/STIX-Web/Normal/Italic/Main.js

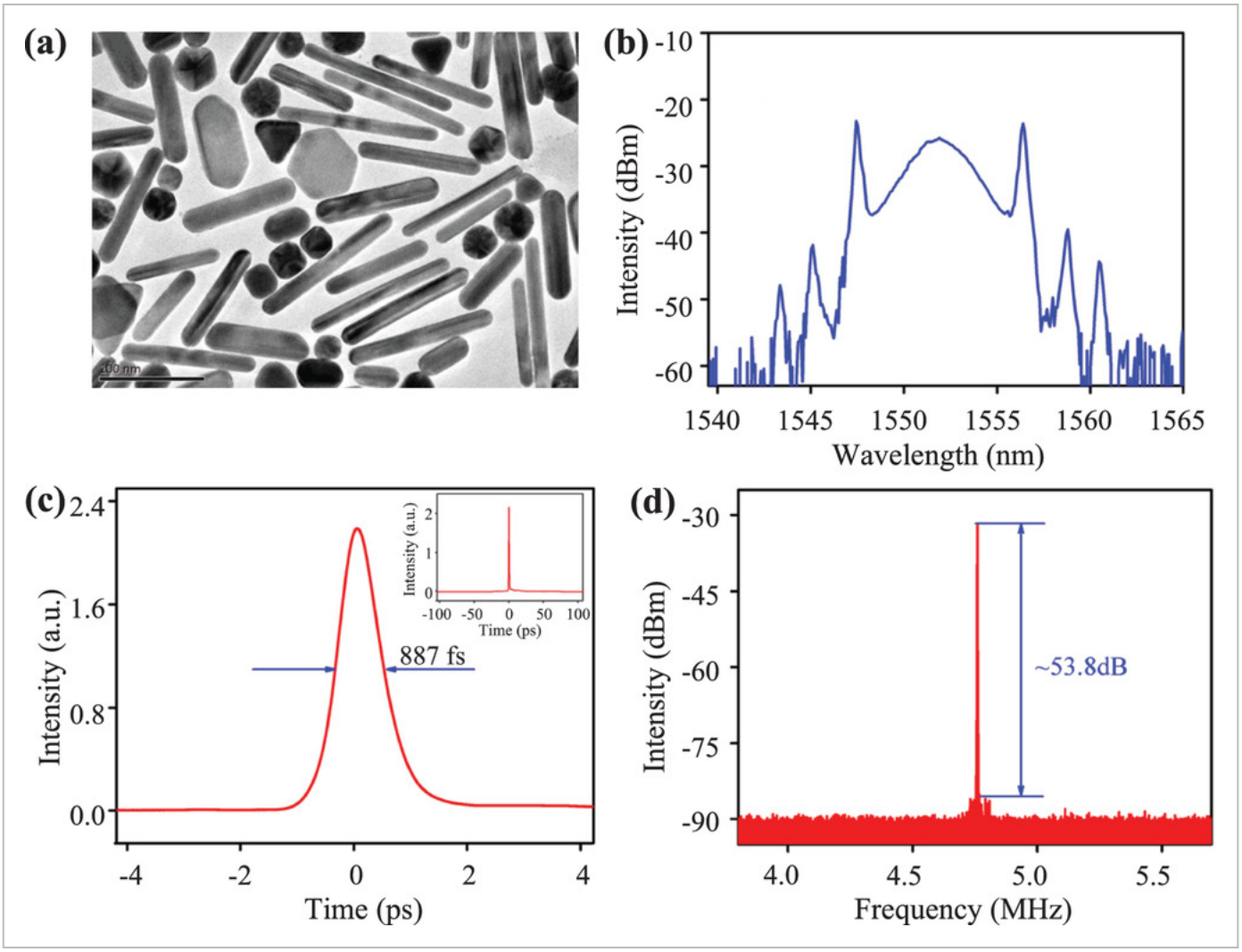

Figure 8

Open in figure viewer | PowerPoint

Mode-locked results of ultrafast pulse based on GNRs. a) TEM image of GNRs. b) Optical spectrum, c) autocorrelation trace, and d) RF spectrum. Reproduced with permission.[95] Copyright 2014, AIP Publishing LLC.

Apart from GNPs and GNRs, demonstrations on the use of G-NBPs and GNWs as SAs were also reported. In 2017, Zhang et al. investigated a novel diode pumped solid state (Nd, La:SrF_2) laser based on a G-NBPs SA, obtaining a Q-switched pulse with the shortest pulse width of 1.15 μs and the corresponding maximum single pulse energy was 2.24 μJ.[97] In 2021, Luo et al. explored the potential of gold nanowires (GNWs) in mid-infrared application, in which mode-locked laser based on gold nanomaterials and harmonic mode-locking based on material SA were all first obtained in 3-μm band.[189]

4.1.2 Silver

As another type of typical metal nanomaterials, SNPs have also attracted considerable interest due to the large third-order nonlinearity, high electrical and thermal conductivities, as well as

Loading [MathJax]/jax/output/HTML-CSS/fonts/STIX-Web/Normal/Italic/Main.js

easy fabrication.[190-192] Many studies showed that SNPs have the saturable absorption properties required for the construction of ultrafast lasers.[87, 163, 193, 194] In 2015, Guo et al. demonstrated the first realization of ultrafast pulsed output based on a SNPs-SA in an EDFL, where obtained a high-performance Q-switched pulse with maximum single pulse energy of 132 nJ.[82] In 2016, Ahmad et al. firstly reported on a SNPs-based SA for TDFL at 2 μm, in which a highly stable Q-switched pulse with SNR of 59.5 dB was achieved, suggesting the potential for eye-safe applications such as manufacturing and medicine.[195] In 2019, Li et al. proposed an ion implantation method for embedding the SNPs in neodymium-doped YAG crystal to design a monolithic device, in which a Q-switched mode-locked (QM) pulse with a maximum repetition rate of 10.53 GHz was firstly achieved in 1064-nm monolithic waveguide laser.[98] In addition, Rosdin et al. obtained a stable mode-locked pulse by using a SNPs-PVA SA in EDFL, the corresponding SNR of 74.3 dB indicated the stable mode-locking of the pulse.[99] In 2020, Ahmad et al. achieved Q-switched ultrafast pulses in Er- and Tm-doped fiber lasers induced by same Ag-SA thin film, showing that Ag was capable to be a prospect Q-switcher in 1.5- and 2-μm regions.[196] Besides, Fu et al. demonstrated a self-started Q-switched pulse in Yb-doped all-fiber laser, in which a stable and low-cost laser was achieved by using solution-processed SNPTs as SA.[100] **Figure** 9a shows the scanning electronic microscopy (SEM) image of SNPTs deposited on Si substrate. Figure 9b–d exhibits that the 2.59-μs Q-switched pulse has an SNR of 30 dB at the wavelength of 1033.3 nm. In 2021, they also firstly reported a dual-wavelength mode-locked YDFL enabled by SNPTs, where the pulse was centered at 1031.92 and 1033.24 nm. The duration of the mode-locked pulse is 293 ps and the corresponding SNR is 40 dB.[101]

Loading [MathJax]/jax/output/HTML-CSS/fonts/STIX-Web/Normal/Italic/Main.js

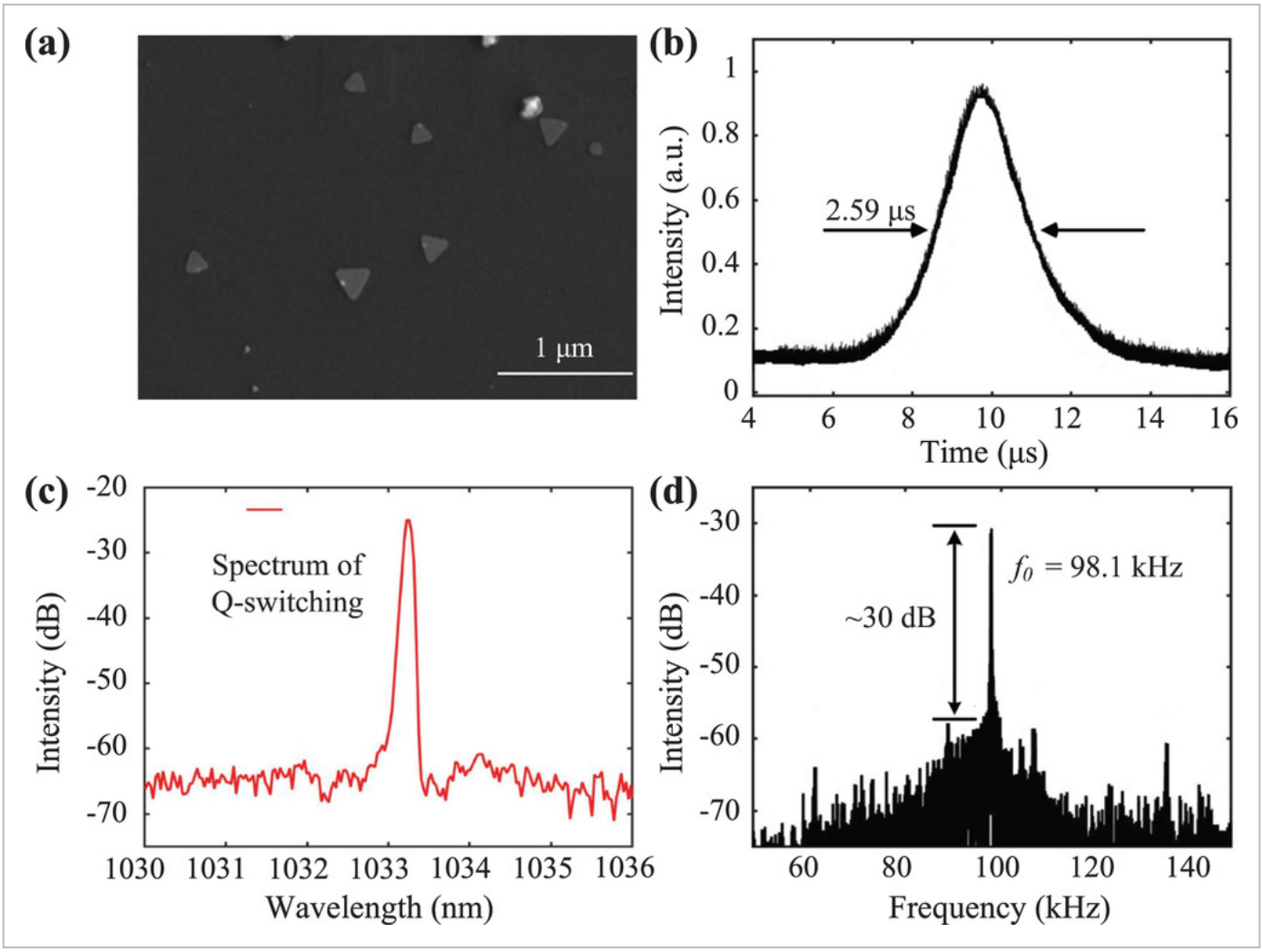

Figure 9

Open in figure viewer | PowerPoint

Q-switched results of ultrafast pulse based on SNPTs. a) SEM image of SNPTs. b) Single pulse profile, c) optical spectrum, and d) RF spectrum. Reproduced under terms of the CC-BY license.[100] Copyright 2020, The Authors, published by De Gruyter.

4.1.3 Copper

In addition to the above-mentioned Au and Ag, Cu is also a reliable SA candidate due to its outstanding optical properties and high cost-effectiveness.[198] In 2016, Wu et al. successfully applied CuNWs-based SA to a Pr-doped ZBLAN fiber laser, achieving a stable Q-switched operation in 635 nm.[132] Subsequently, Muhammad et al. obtained ultrafast pulses in Yb-, Er-, and Tm-doped fiber lasers based on CuNPs, also proving the saturable absorption capability of Cu nanomaterials in 1-, 1.5-, and 2-μm bands, respectively.[104, 199, 200] In order to enhance the nonlinear optical properties of Cu-based SA, CuNPs can be embedded into crystals. In 2019, Wang et al. proposed Q-switched mode-locked waveguide laser in 1064 nm with the repetition rate up to 8.6 GHz, in which the CuNPs were embedded into lithium niobate crystal to be SA.

Loading [MathJax]/jax/output/HTML-CSS/fonts/STIX-Web/Normal/Italic/Main.js

[106] Pang et al. also combined CuNPs with lithium tantalate crystal to generate Q-switched mode-locked pulse in 1-µm waveguide laser.[105] These results indicated the broad application prospects of CuNPs embedded into crystals. In addition, Ismail et al. used CuNPs combined with PVA and chitosan as medium to produce ultrafast pulses in EDFLs, where stable Q-switched pulses with SNRs up to 54 and 71 dB were obtained separately.[102, 201] In 2020, they also demonstrated the realization of soliton mode-locked pulses in an EDFL, which was achieved by CuNWs-SA based on a polydimethylsiloxane (PDMS) polymer.[103] In 2021, Muhammad et al. fabricated CuNPs by using E-beam deposition method and integrated it into laser cavity through PVA polymer as a carrier.[197] **Figure** 10a shows the TEM image of nanoscale CuNPs. Based on this SA, mode-locked pulse centered at 1564.3 nm with the pulse width of 2.85 ps and high SNR of 71 dB was achieved, as shown in Figure 10b–d. Up to now, ultrafast lasers based on Cu nanomaterials have been widely reported with different forms including CuNWs, CuNPs, and Cu pellets, proving their potential for applications in ultrafast photonics.

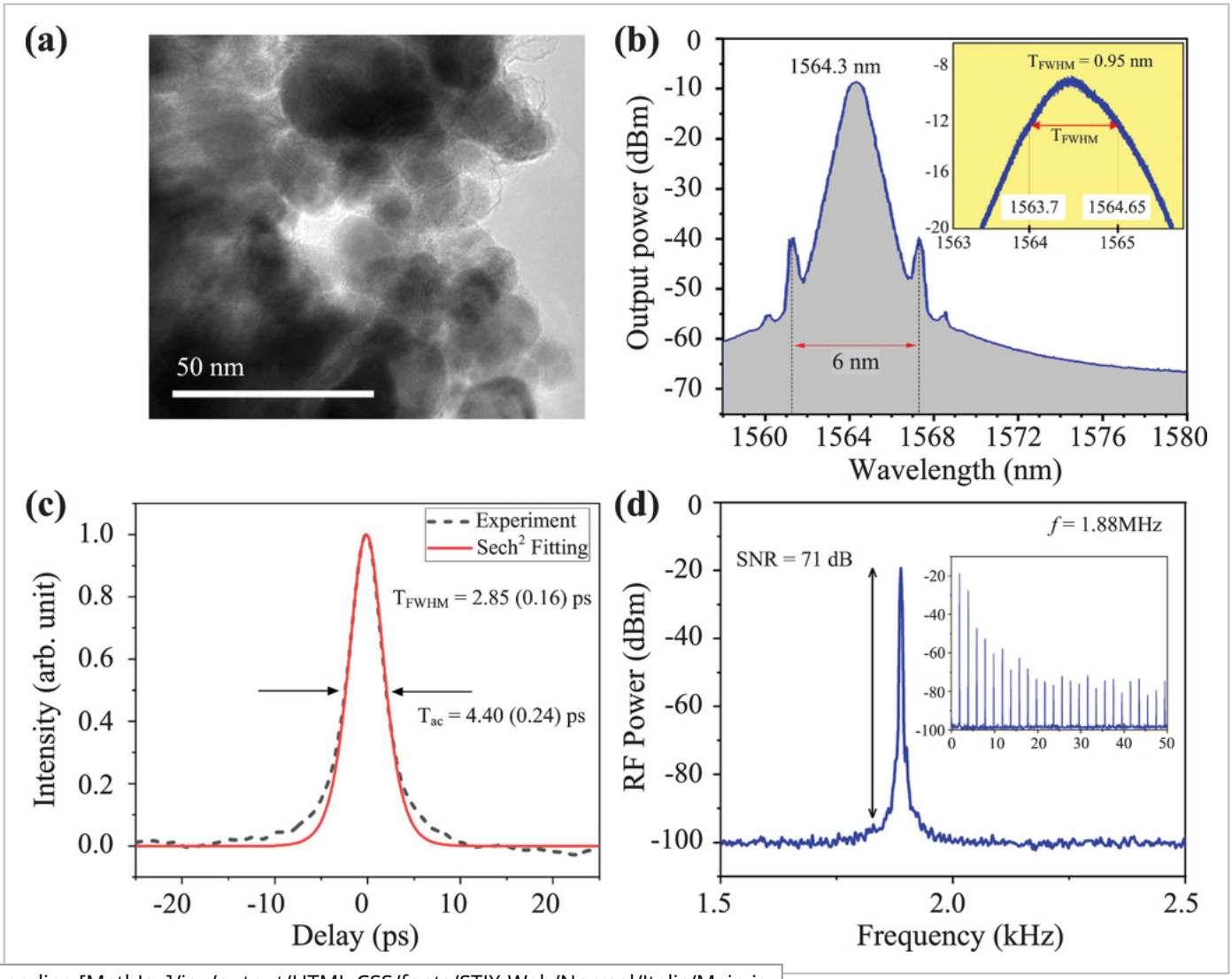

Loading [MathJax]/jax/output/HTML-CSS/fonts/STIX-Web/Normal/Italic/Main.js

Figure 10

Open in figure viewer | PowerPoint

Mode-locked results of ultrafast pulse based on CuNPs. a) TEM image of CuNPs. b) Optical spectrum, c) single pulse profile, and d) RF spectrum at 2.5 kHz and 50 MHz resolution. Reproduced with permission.[197] Copyright 2021, Elsevier Ltd.

4.2 Metal-Oxide Nanoparticles

4.2.1 Transition Metal Oxides

As novel metal oxides, transition metal oxides (TMOs) are favorable for applications in ultrafast photonics due to their excellent optical properties.[169, 202] Moreover, TMOs are zero-dimensional materials with smaller lateral size and regular circle-like shape, which allow them to be prepared more uniform.[84, 145, 203] Recently, ultrafast lasers enabled by typical TMOs such as Fe_3O_4, ZnO, and TiO_2 have been investigated and reported, indicating the capacity of TMOs in generating ultrafast pulses.

FONPs are commonly used zero-dimensional TMOs, which have high nonlinear optical absorption and fast recovery time.[170, 204] In addition, FONPs also possess semiconductor properties and bandgap that can be tuned by changing the diameter of the nanoparticles [6-8]. Therefore, FONPs are considered as promising nonlinear optical materials and gradually used as SAs in ultrafast photonics. Furthermore, Fe_2O_3 often is the end product of the transformation of other iron oxides, and it also has excellent saturable absorption property that can be applied to ultrafast lasers.[204] In 2016, Bai et al. realized passively Q-switched operation in EDFL by using an SA based on FONPs for the first time, in which the FONPs were derived from the magnetic fluid.[84] In 2017, Mao et al. fabricated two kinds of SAs to obtain Q-switched pulses by embedding FONPs into PVA and polyimide films, respectively, where polyimide-based SA exhibited stronger laser power tolerance due to its higher fusion point.[203] Chen et al. also reported the single- and multi-wavelength Q-switched fiber laser using FONPs as SA.[205] These results all proved that FONPs can act as effective Q-switcher at 1.5-μm band. Subsequently, Wang et al. demonstrated that FONPs could be applied to 1-μm band, and achieved a passively Q-switched Nd:YVO_4 solid state laser for the first time.[145] Then, Koo et al. investigated the potential of FONPs as an SA in 2-μm band for the first time by using Fe_3O_4/PVA-composite as SA, in which a Q-switched pulse with a SNR up to 51 dB was obtained.[206] In 2018, Liu et al. also realized a Q-switched operation with a maximum pulse energy of 4.9 μJ in 2-μm Tm:Lu_3Al_5O 12 bulk laser.[207] Al-Hayali et al. proposed a dual-wavelength passively Q-switched Yb-doped fiber laser based on FONPs-SA by adjusting the pump power and polarization controller state.[208] Besides, Mao et al. fabricated Fe_2O_3 NPs-SA based on PVA composite and applied it to generate Q-switched pulses in Yb-, Er-, and Tm-doped fiber lasers, respectively. Q-switched cylindrical vector beams with spatial-structured polarization state were [illegible] laser, which can be attributed to

Loading [MathJax]/jax/output/HTML-CSS/fonts/STIX-Web/Normal/Italic/Main.js

the insensitive polarization state of Fe_2O_3.[110] While many groups have used FONPs SA to implement Q-switched operation, only a few papers reported the mode-locked laser with FONPs as SA.[209] Therefore, in 2019, Li et al. exploited FONPs as SA to achieve mode-locked operation at 1558 nm, confirming the feasibility of FONPs as mode locker.[108] Wang et al. presented a stable mode-locked EDFL with SNR of 67 dB, which was enabled by a novel FONPs-SA formed by using the mode coupling property of excessively tilted fiber grating.[210] In 2020, the first demonstration of FONPs-based SA for ultrafast laser at 3 μm was reported. Yang et al. obtained a Q-switched pulse in a tunable Dy-doped ZBLAN fiber laser, suggesting that FONPs was a promising kind of SA material for mid-infrared region.[211] Besides, Chen et al. and Cheng et al. observed Q-switched mode-locked phenomena in Yb- and Er-doped fiber laser by increasing the pump power and adjusting the state of PC, in which the value of FONPs for QM fiber laser was exhibited.[212, 213] Ma et al. achieved mode-locked pulse in a 1064-nm solid-state laser using FONPs-based SA, where the maximum average output power of 856 mW with pulse energy of 6.85 nJ was obtained at the pump power of 11 W.[109] In 2021, Li et al. reported on the broadband nonlinear properties of Fe_3O_4 in triple-wavelength bands, where passive Q-switched pulses operated at 1039, 1560, and 1982 nm were achieved, respectively.[214] **Figure** 11a shows the TEM and SEM images of FONPs with an average diameter of 20 nm on 100- and 200-nm scales. As a representative of broadband results, the optical spectrum, pulse profile, and RF spectrum in 2 μm are shown in Figure 11b–d. These Q-switched pulses in different bands based on the same FONPs-SA all indicated its ability to perform in broadband applications.

Loading [MathJax]/jax/output/HTML-CSS/fonts/STIX-Web/Normal/Italic/Main.js

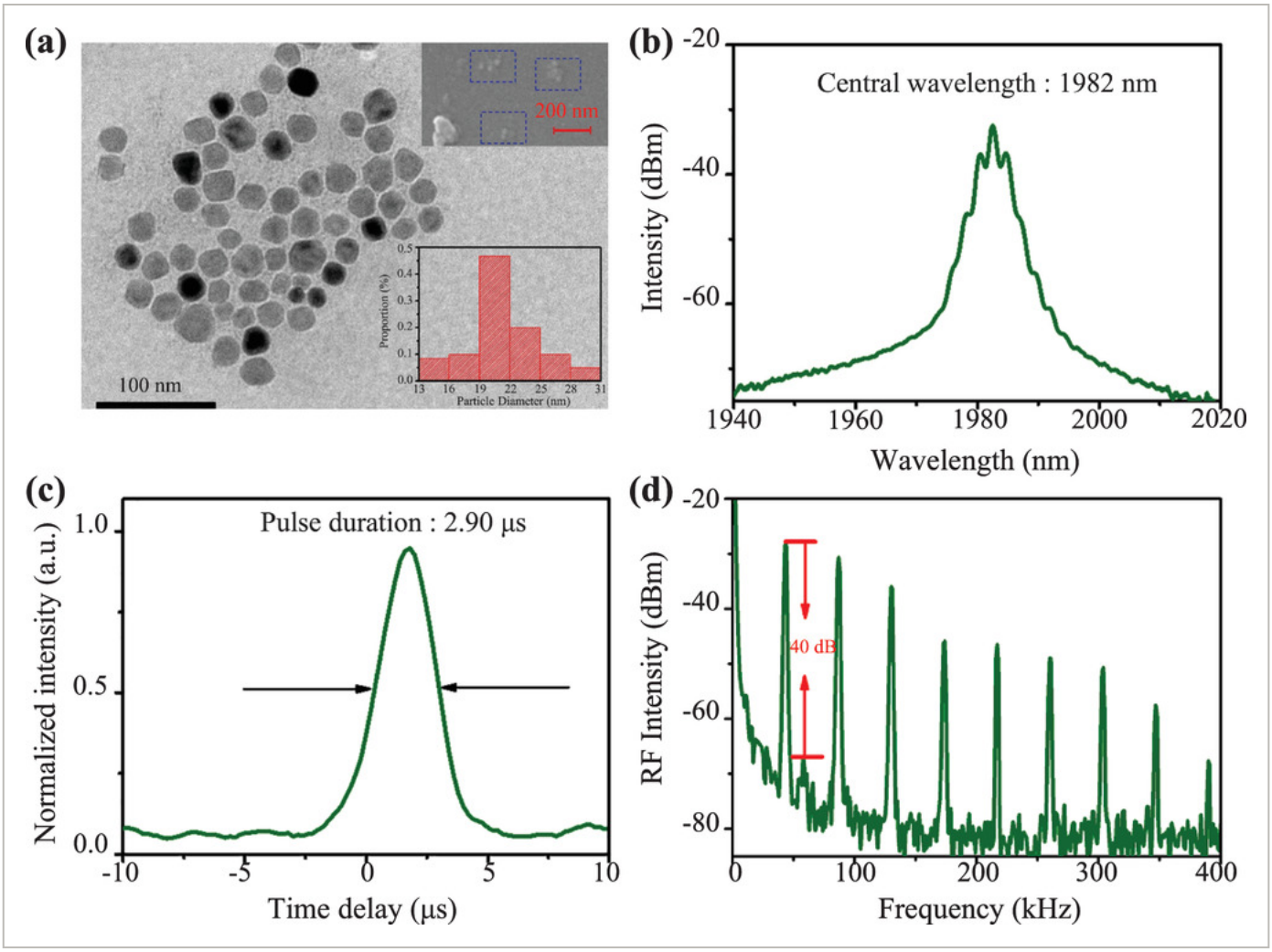

Figure 11

Open in figure viewer | PowerPoint

Q-switched results of ultrafast pulse based on FONPs. a) TEM image of FONPs (inset: SEM image and diameter distribution). b) Optical spectrum, c) pulse profile, and d) RF spectrum. Reproduced with permission.[214] Copyright 2021, Elsevier Inc.

ZnO is a kind of typical TMO material that has outstanding optical and electrical properties, making it attractive for various practical applications. For example, due to the large bandgap (3.37 eV) and high binding energy (60 meV), ZnO has been widely used for devices in UV spectral range.[171, 215, 216] In addition, ZnO has advantages of high third-order nonlinear absorption coefficient and short recovery time, which fulfill the requirements of SA materials in ultrafast lasers.[151, 217] In 2016, Ahmad et al. first demonstrated the saturable absorption of ZnO in an EDFL, where Q-switched pulse with 47.9-nJ high pulse energy was obtained.[85] Subsequently, they also explored the ability of ZnO to generate ultrafast pulse in 1-μm band, in which a stable Q-switched YDFL was achieved, corresponding to an SNR of 53 dB.[218] In 2017, Aziz et al. reported on Q-switched pulses in an EDFL enabled by ZnO-PVA film.[219] The pulse

Loading [MathJax]/jax/output/HTML-CSS/fonts/STIX-Web/Normal/Italic/Main.js

ere 7 μs and 154.6 nJ, respectively.

The above results proved that ZnO is a promising SA candidate for ultrafast lasers, but mode-locked pulses had not been investigated. In 2018, Alani et al. proposed the first mode-locked EDFL by using ZnO as SA, where the self-started pulses were generated with a 2.6-ps width at the repetition rate of 3.26 MHz.[220] In 2019, Husin et al. integrated ZnO-SA into an EDFL as Q-switcher, in which the 0.46-mW output power and 18.13-nJ pulse energy were received at the maximum pump power of 48.58 mW.[221] Moreover, a ZnO SA was also applied to a laser in 2-μm band that is beneficial to eye-safe applications, including spectroscopy and medicine. Ahmad et al. demonstrated a mode-locked TDFL using ZnO as SA, the pulse width at the repetition rate of 11.36 MHz was measured to be 1.395 ps.[111] Recently, Muhammad et al. first used ZnO/PDMS composite based on a tapered fiber as mode-locker, in which 1.03-ps pulses were obtained in 1558 nm, indicating the ability of ZnO/PDMS-clad taper fiber to generate ultrafast pulses.[222]

TiO_2 is also a desirable SA candidate that exhibits 1.5-ps ultrafast recovery time at room temperature, large modulation depth up to 35.41%, and excellent nonlinear optical properties.[86, 178, 223] Although TiO_2 has a larger bandgap of 3.2 eV, the spectral absorption can cover the range from visible to near-infrared regions, which is relative to the crystal form and particle size.[149, 224-226] In 2016, Ahmad et al. investigated the potential of TiO_2 as SAs, where Q-switched pulses were achieved in both 1- and 1.5-μm bands, indicating the ability to generate ultrafast pulses.[86, 227, 228] In 2017, they combined TiO_2 and PVA film, as well as sandwiched them into laser cavity. The first mode-locked operation based on TiO_2 was demonstrated in Tm-Ho co-doped fiber laser, corresponding to the output power and pulse energy of 62 mW and 1.66 nJ, respectively.[116] However, the PVA polymer film has a low melting point and the damage to SAs in sandwich structure is relatively large at high pump power. Therefore, in 2018, Reddy et al. proposed an EDFL enabled by TiO_2-doped fiber, which achieved stable mode-locked pulses with an SNR of 54 dB.[229] In 2019, Rahman et al. also investigated the ability of TiO_2-doped fiber to generate ultrafast pulse in 1- and 1.5-μm lasers, where high pulse energies of 191 and 8.56 nJ were obtained, proving the feasibility of TiO_2-doped fiber for high-power applications.[230, 231] Subsequently, Wang et al. realized the first Q-switched solid-state laser based on TiO_2 film SA. The maximum output power and pulse energy can reach up to 2.35 W and 1.17 μJ at the repetition rate of 2.008 MHz.[232] In 2020, Yusoff et al. deposited TiO_2 polymer composite onto tapered microfiber as SA, in which Q-switched operation was achieved at a low threshold of 16 mW.[117]

In recent years, some novel TMOs such as NiO, CuO, and V_2O_5 have also attracted considerable attention in applications of ultrafast lasers. The nonlinear optical properties of NiO have been studied by Z-scan technique, which proved its saturable and two-photo absorption properties.[233] Therefore, in 2017, Nady et al. first used NiO NPs as SA for an EDFL, where Q-switched [illegible] tential for the generation of

Loading [MathJax]/jax/output/HTML-CSS/fonts/STIX-Web/Normal/Italic/Main.js

ultrashort pulses.[113] In 2018, the first demonstration of mode-locked EDFL based on NiO was reported by Harun et al., which realized self-starting pulse at repetition rate of 1.1 MHz.[234] Subsequently, Al-Masoodi et al. explored the saturable absorber properties of NiO in 1-μm band, in which passive mode-locked and Q-switched pulses were both observed, confirming that NiO is a promising SA candidate for ultrafast laser.[112] In 2019, Rusdi et al. also proposed Q-switched and mode-locked pulses generated from TDFL enabled by NiO film SA for the first time.[235] Q-switched pulses were achieved while mode-locked pulses were realized successively by controlling the dispersion and nonlinearity of laser cavity. As for CuO nanomaterials, the higher optical nonlinearities than Cu nanoparticles make them more suitable as SA candidates.[152, 236] Moreover, CuO has a bandgap around 1–2 eV that is smaller than other TMOs, such as ZnO (3.37 eV) and TiO_2 (3.2 eV), indicating its superiority for applications in NIR.[215, 225, 237] In 2018, Sadeq et al. investigated the ability of CuO nanomaterial for generating ultrashort pulses, in which Q-switched and mode-locked operations were first achieved in EDFLs, respectively.[115, 238] In 2020, Al-Masoodi et al. established a Q-switched laser centered at 1035.4 nm using CuO NPs as SA; the relatively high pulse energy of 0.192 μJ was obtained corresponding to an average output power of 20 mW.[114] It was also the first realization of Q-switched YDFL based on CuO nanomaterial. V_2O_5 is the most important and stable one among several vanadium oxides, whose nonlinear optical properties have also been explored.[239, 240] In 2018, Nady et al. investigated the abilities of V_2O_5 as Q-switcher and mode-locker in ultrafast lasers, where desirable Q-switched and mode-locked pulses were both obtained in 1.5-μm band.[118, 119] Meanwhile, Rahman et al. exploited V_2O_5-SA to generate Q-switched pulses at the wavelength of 1968 nm, where the maximum output pulse energy was 154.92 nJ.[241] Very recently, Rizman et al. realized a Q-switched EDFL based on V_2O_5 SA that was integrated into laser cavity by using a polymer composite, corresponding to a tunable wavelength range of 30 nm.[120] These results showed that V_2O_5 can be a reliable SA material for applications in ultrafast photonics.

4.2.2 Other Metal Oxides

In addition to the above TMOs, some other metal oxides with outstanding nonlinear properties also deserved to be explored. In 2016, Alam et al. revealed that ITO can obtain excellent intensity-dependent refractive index and ultrafast response time of 360 ps.[242] ITO also has broadband operation regions due to the tunable plasmonic absorption peak from 1600 to 2200 nm, which can be achieved by changing the doping concentration of tin.[243, 244] Thus, ITO has been gradually studied as a promising SA candidate. In 2017, Guo et al. used ITO NPs as SAs, and a passive Q-switched pulse was demonstrated in an EDFL.[121] The ITO NPs were fabricated by coprecipitation method. TEM image and particle size distribution for ITO are shown in **Figure** 12a. Figure 12b exhibits the high resolution TEM image, in which the lattice fringe prove the high quality of the ITO nanocrystals. Figure 12c,d shows the Q-switched pulse with pulse width of 1.742 μs and optical spectrum centered at 1530.3 nm. Subsequently, in 2018, they

Loading [MathJax]/jax/output/HTML-CSS/fonts/STIX-Web/Normal/Italic/Main.js

dropped ITO colloidal liquid based on PVA between two fiber connectors, in which the first dark soliton pulse enabled by ITO was firstly obtained in EDFL.[122] Moreover, other methods for integrating ITO into laser cavity as SA have also been investigated. In 2020, Nizamani et al. used D-shaped fiber-based ITO SAs as media to achieve ultrafast lasers, in which mode-locked and Q-switched EDFLs were both established, indicating the potential of applications in ultrafast photonics.[123-125] In recent years, PbO and MgO have also attracted growing attention due to their excellent optical properties. MgO has high optical transparency, fast recovery time, high temperature stability, and low cost that make it popular in ultrafast optics.[245, 246] As an oxide, PbO possesses high stability in air. The nonlinear optical properties of PbO were also investigated, proving the potential for ultrafast applications. In 2019, Khaleel et al. applied MgO-PVA thin film as SAs in laser cavity, where a mode-locked EDFL with 5.6-ps pulse width and 50-dB SNR was demonstrated.[247] Song et al. used PbO nanosheets as SAs that were integrated by sandwiching between two connectors of fiber or decorating on a microfiber.[248] It was observed that mode-locked pulses centered at 1- and 1.5-μm bands were both generated, respectively. These results above indicated that metal oxides can play important roles in applications of ultrafast photonics and further promote the development of ultrafast lasers.

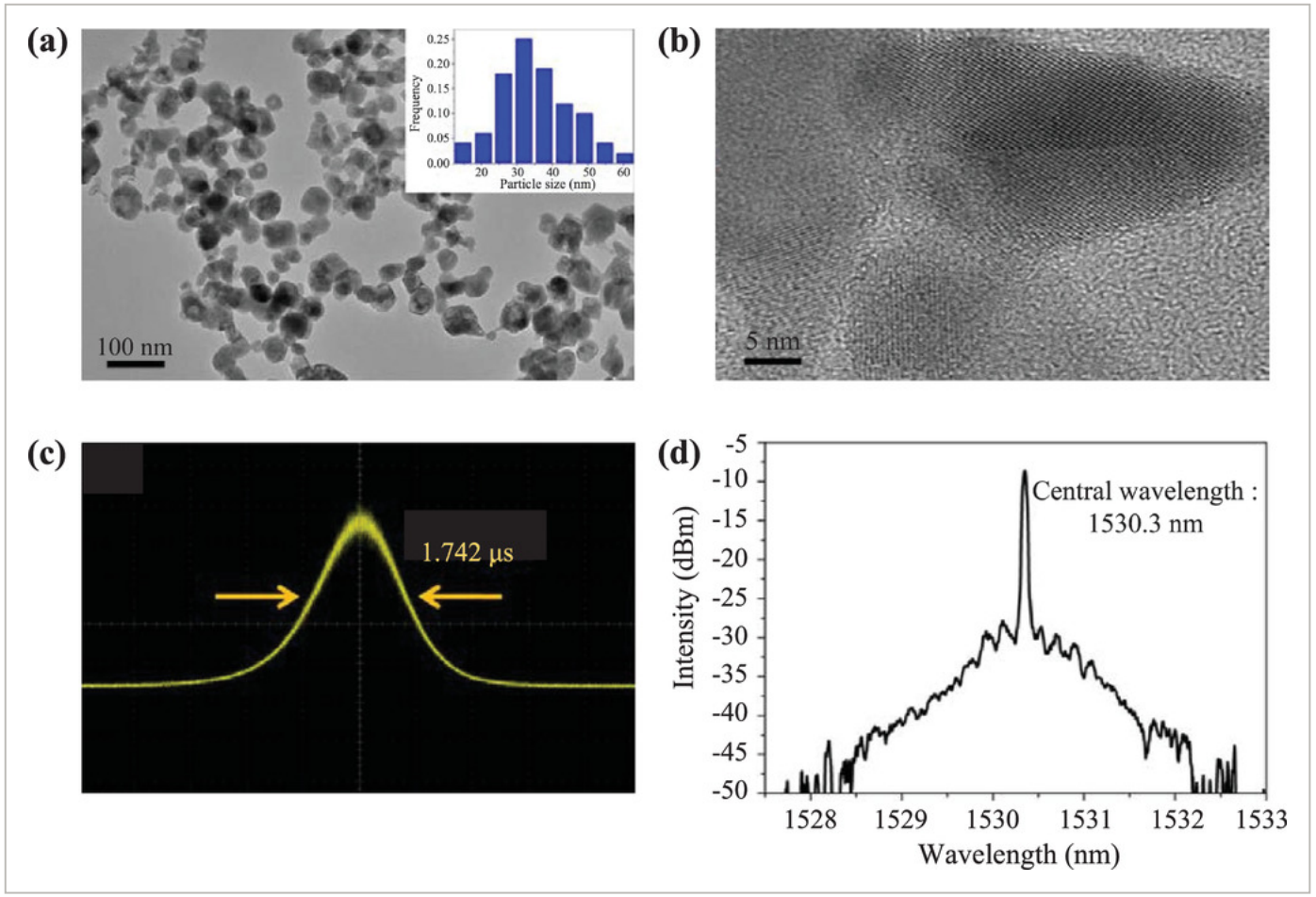

Figure 12

Loading [MathJax]/jax/output/HTML-CSS/fonts/STIX-Web/Normal/Italic/Main.js

Open in figure viewer | PowerPoint

Q-switched results of ultrafast pulse based on ITO NPs. a) TEM image of ITO NPs (inset: particle size distribution). b) HRTEM image of ITO NPs. c) Single pulse profile and d) optical spectrum of the Q-switched pulse. Reproduced with permission.[121] Copyright 2017, Optical Society of America.

Metal-based nanomaterials are generally exploited as SAs to construct Q-switched and mode-locked pulses in lasers. Strongly enhanced SPR at the optical frequency of MNPs strengthen their excellent properties, especially nonlinear optical properties. In addition, different forms of nanoparticles such as nanorods, nanoplates, nanowires, and so on also have crucial effects on their properties and applications. **Table** 2 summarizes visualized data of lasers that are enabled by different metal-based nanomaterials, gain media, and regimes. It is observed that the threshold of ultrafast operation can be as low as 8 mW, indicating the potential of nanomaterials as SAs in lasers. Moreover, the duration and repetition rate of pulses enabled by metal-based nanomaterials can reach to the level of fs and GHz, which are desirable for applications such as micromachining and medical treatment.[249, 250] However, the existing results of ultrafast lasers are mostly in 1- and 1.5-μm bands, while research in farther bands is still inadequate. Similar to MNPs, most MONPs including the typical TMOs also have large bandgaps, limiting their abilities in broadband operations. However, the spectral absorption can be broadened by controlling the crystal forms and particle size of oxides. Moreover, the fast recovery time, high modulation depth, and low saturable intensity of MONPs are also desirable properties for SA materials.

Table 2. Summary of typical ultrafast lasers enabled by diverse metal-based nanomaterials

SA devices *a)*					Laser parameters *b)*		
Material	**Integration**	**Gain Medium**	**Regime**	**Thres-hold**	**λ [nm]**	**τ [s]**	**f r e**
GNPs	NaCMC	Er	QS	30	1560	3.2 μ	24.2
GNPs	PVA	Pr-doped ZBLAN	QS	126.3	635	556−235 n	285 k
GNPs	PMMA	TDFF	ML	–	1506.26	4.04 p	6.89
GNPs	Ion sputtering	Er-doped ZBLAN	QS	3.52 W	2780	0.81−3.713 μ	22.9 k
GNPs	PVA	Er	ML	157	1561	436 n	1 M

Loading [MathJax]/jax/output/HTML-CSS/fonts/STIX-Web/Normal/Italic/Main.js

SA devices [a]					Laser parameters [b]		
Material	Integration	Gain Medium	Regime	Thres-hold	λ [nm]	τ [s]	f r e
GNRs	NaCMC	Er	QS	27	1560	4.8−23 μ	7.1
GNRs	EF	Er	ML	52	≈1552	≈887 f	4.7

a) Materials: gold nanorods (GNRs), nanowires (NWs), nanoparticles (NPs), nanobipyramids (NBPs), silver nanoparticles (SNPs), nanoplates (NPTs), copper (Cu), ferroferric oxide (Fe_3O_4), Fe_3O_4 nanoparticles (FONPs), ferric oxide (Fe_2O_3), zinc (Zn), titanium (Ti), nickel (Ni), vanadium (V), Indium (I), tin (T), magnesium (Mg), lead (Pb); Intergation: sodium carboxymethylcellulose (NaCMC), evanescent field (EF), polyvinyl alcohol (PVA), optical deposition (OD), poly methyl-methacrylate (PMMA), lithium niobate ($LiNbO_3$), lithium tantalate ($LiTaO_3$), polydimethylsiloxane (PDMS), polyimide (PI), deposited onto the surface of fiber ferrule (DSFF), polyethylene oxide (PEO), N-methyl-2-pyrrolidone (NMP), polyethylene glycol (PEG)

b) Gain medium: erbium (Er), ytterbium (Yb), thulium (Tm), holmium (Ho), praseodymium (Pr), ZrF_4-BaF_2-LaF_3-AlF_3-NaF (ZBLAN), neodymium (Nd), lanthanum (La), thulium-doped fluoride fiber (TDFF), strontium (Sr), fluorine (F), yttrium aluminum garnet (YAG), lutetium (Lu), dysprosium (Dy); Regime: Q-switching (QS), Mode-locking (ML), Q-switched mode-locking (QSML); wavelength (λ); pulse width (τ); signal to noise ratio (SNR); repetition rate (f_{rep}).

5 Perspectives

The remarkable optical properties exhibited by both MNP and MONP allow covering a broad range of wavelengths in visible and near-infrared regions just by tuning intrinsic particle properties such as size and geometry. This is a strong advantage for these materials that will continue expanding the range of wavelengths covered and laser type used. From an SA fabrication standpoint, there are mainly hybrid (chemical/physical) methods that have been successfully demonstrated for the production of NPs. But these methods have not yet been proposed for SA fabrication that may find a space in the future. As an example, NPs can be easily produced in the spherical form by the laser ablation in liquids method, which consists of the generation of NPs in a liquid owing to the action of a laser focused on a target of the related material.[251] This method allows wide flexibility in terms of materials and solvents, because any target can be used, and the procedure can be carried out in any liquid. Moreover, it does not need any chemical and the final NPs have thus very high purity. It has also been demonstrated that anisotropic MNPs can be obtained by laser ablation in liquids itself[252] or by light

Loading [MathJax]/jax/output/HTML-CSS/fonts/STIX-Web/Normal/Italic/Main.js

or by laser ablation in liquids.[254,

255] Furthermore, a variety of green methods have also been proposed, which exploit a range of natural agents like plant extracts, bacteria, algae, etc. for both stabilization and reaction.[256] Such methods do not involve the use of synthetic chemicals and can contribute to knocking down the environmental footprint of NP synthesis.

As for the applications in ultrafast photonics, nanomaterial-based SAs have been widely used owing to the various outstanding properties. The use of graphene in ultrafast lasers paves the way for the application of 2D materials. Graphene has ultrafast recovery time, high electron mobility, and broadband responses, but the single-layer transmittance is only 2.3%, affecting its wide use in optical modulation. TIs have small bandgap that makes them promising candidates for broadband operation. However, the complex absorption mechanism and fabrication process are also limitations in practical uses. The bandgap of TMDs can be tuned by changing the number of layers, but the direct bandgap of monolayer is 1.9 eV, leading to the absorption band far from the mid-infrared region. BP possesses broadband nonlinear response and tunable bandgap, whereas it is relatively unstable in air so that other storage or protection methods are required. As a kind of novel 2D material, MXenes have attracted considerable research interest on account of the excellent optical properties, but the studies of applications based on more kinds of materials and in farther bands are still in the early stage. When it comes to metal-based nanomaterials, the properties of large nonlinear coefficient, fast recovery time, and excellent saturable absorption also need to be highlighted, but the control of optical properties of metal nanomaterials can be further investigated. In order to satisfy different requirements, the nonlinear optical response and absorption band can be controlled by changing shapes or optimizing aspect ratio. Besides, MNPs also have strong photothermal effect,[257] in which the heat accumulation makes them damaged when laser is operated at high power or for a long time. Therefore, the use of D-shaped or tapered fibers combined with MNPs to form SA is significant because evanescent field can greatly decrease the direct contact area of coupling between the signal light and SAs. The damage threshold of MNPs can be enhanced while ensuring the saturable absorption. MONPs have preferable stability in the air whereas they are difficult to prepare. For example, oxygen vacancy defects will appear in the preparation of TMOs. However, it is shown that new energy levels can be generated with the defects of oxygen vacancy as donors, which decreases the bandgap of TMOs.[258, 259] Furthermore, Ti^{4+} in TiO_2 has been proved to bring more oxygen vacancy defects, which is a promising direction to make up the shortcoming of large bandgap, thereby expanding applications of nanomaterials in mid-infrared regions.[260, 261] Moreover, metal-based nanomaterials also have potential in further optical applications. For example, optical amplifier is required for wavelength-division-multiplexing transmission systems in optical communication, where metal nanoparticles (MNPs) doped with other materials act as superior gain medium.[262, 263] In addition, benefiting from the excellent localized SPR, light confined to

Loading [MathJax]/jax/output/HTML-CSS/fonts/STIX-Web/Normal/Italic/Main.js cules in a few tens of nanometers,

making metal-based nanomaterials highly competitive in the field of high-resolution imaging. [264, 265]

6 Conclusions

The outstanding properties of large third-order nonlinear absorption coefficient, ultrafast recovery time, and superior SPR enable metal-based nanomaterials attractive for ultrafast photonics. The intention of this review is to summarize the state of the art of metal-based nanomaterials, including synthesis methods, optical properties, and applications in ultrafast lasers. Therefore, we introduce the typical preparation methods that can influence the properties of metal-based nanomaterials from the view of physical and chemical methods. Then we focus on the excellent optical properties of MNPs and MONPs, respectively. Especially, the nonlinear optical properties of all metal-based nanomaterials are discussed. Furthermore, we summarize the typical mode-locked and Q-switched results based on various metal-based nanomaterials from their first demonstration in ultrafast lasers to the most recent. Finally, the easier preparation methods and superior optical properties of metal-based nanomaterials are also prospected to promote their better applications in ultrafast photonics. It is believed that the exploration for materials with excellent performance always brings new technological revolutions and further accelerates the update of various devices.

Acknowledgements

This work was supported by Beijing Natural Science Foundation (4202044); National Natural Science Foundation of China (62071016); Fundamental Research Funds for the Central Universities; Open Fund of IPOC (BUPT); and State Key Laboratory of Luminescence and Applications (SKLA-2020-03).

Conflict of Interest

The authors declare no conflict of interest.

Biographies

Loading [MathJax]/jax/output/HTML-CSS/fonts/STIX-Web/Normal/Italic/Main.js

Bo Fu received his Ph.D. degree from Tsinghua University in 2015. After 2 years research in University of Cambridge, he began his independent career as an associate research professor in Beihang University. He has authored and co-authored more than 60 peer-reviewed papers. His research interests include ultrafast lasers, nanophotonics, nanomaterials, etc.

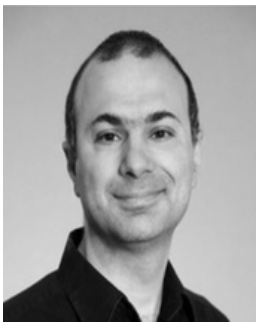

Vittorio Scardaci received the Laurea (B.S. and M.S.) degree in chemistry from the University of Catania, Catania, Italy, in 2004, and the Ph.D. degree in engineering from the University of Cambridge, Cambridge, UK, in 2009. He spent 10 years as R&D Scientist with Hewlett-Packard, Ireland, before joining the University of Catania as a lecturer in physical chemistry in 2018. His research interests include the synthesis, characterization, and application of carbon-based and silver-based nanomaterials.

Han Zhang received his B.S. degree from Wuhan University in 2006 and Ph.D. degree from Nanyang Technological University in 2010. He is currently professor and director of Shenzhen Engineering Laboratory of Phosphorene and Optoelectronics, Shenzhen University, China. He is a Fellow of Royal Society of Chemistry (RSC) and a Fellow of Optical Society of America (OSA). His current research focuses on photonics of low-dimensional materials and devices.

References

1 S. Liu, Z. Tang, *J. Mater. Chem.* 2010, **20**, 24.
Crossref | CAS | PubMed | Web of Science® | Google Scholar

Loading [MathJax]/jax/output/HTML-CSS/fonts/STIX-Web/Normal/Italic/Main.js

3, 6156.

Crossref | CAS | Web of Science® | Google Scholar

3 P. Han, W. Martens, E. R. Waclawik, S. Sarina, H. Zhu, *Part. Part. Syst. Charact.* 2018, **35**, 1700489.
Wiley Online Library | Web of Science® | Google Scholar

4 I. Capek, *Noble Metal Nanoparticles: Preparation, Composite Nanostructures, Biodecoration and Collective Properties*, Springer, Tokyo, Japan 2017, pp. 125– 210.
Crossref | Google Scholar

5 D. A. Vanden Bout, *J. Am. Chem. Soc.* 2002, **124**, 7874.
Crossref | CAS | Web of Science® | Google Scholar

6 A. Trügler, *Optical Properties of Metallic Nanoparticles*, Springer, Cham, Switzerland 2011.
Google Scholar

7 Y. He, Y. Miao, C. Li, S. Wang, L. Cao, S. Xie, G. Yang, B. Zou, C. Burda, *Phys. Rev. B* 2005, **71**, 125411.
Crossref | CAS | Web of Science® | Google Scholar

8 D. M. Sherman, T. D. Waite, *Am. Miner.* 1985, **70**, 1262.
CAS | Web of Science® | Google Scholar

9 U. Keller, *Nature* 2003, 831.
Crossref | PubMed | Web of Science® | Google Scholar

10 M. Qiu, D. Wang, W. Liang, L. Liu, Y. Zhang, X. Chen, D. K. Sang, C. Xing, Z. Li, B. Dong, F. Xing, D. Fan, S. Bao, H. Zhang, Y. Cao, *Proc. Natl. Acad. Sci. U. S. A.* 2018, **115**, 501.
Crossref | CAS | PubMed | Web of Science® | Google Scholar

11 V. Letokhov, *Nature* 1985, **316**, 325.
Crossref | CAS | PubMed | Web of Science® | Google Scholar

12 B. Fu, C. Zhang, W. Lyu, J. Sun, C. Shang, Y. Cheng, L. Xu, *Appl. Spectrosc. Rev*. DOI: 10.1080/05704928.2020.1857258.
Google Scholar

13 J. Zheng, Z. Yang, C. Si, Z. Liang, X. Chen, R. Cao, Z. Guo, K. Wang, Y. Zhang, J. Ji, *Acs Photonics* 2017, **4**, 1466.
Crossref | CAS | Web of Science® | Google Scholar

14 O. Okhotnikov, A. Grudinin, M. Pessa, *New J. Phys.* 2004, **6**, 177.

Loading [MathJax]/jax/output/HTML-CSS/fonts/STIX-Web/Normal/Italic/Main.js

15 V. Matsas, T. Newson, D. Richardson, D. N. Payne, *Electron. Lett.* 1992, **28**, 1391.
Crossref | Web of Science® | Google Scholar

16 N. Doran, D. Wood, *Opt. Lett.* 1988, **13**, 56.
Crossref | CAS | PubMed | Web of Science® | Google Scholar

17 C. Aguergaray, N. G. Broderick, M. Erkintalo, J. S. Chen, V. Kruglov, *Opt. Express* 2012, **20**, 10545.
Crossref | CAS | PubMed | Web of Science® | Google Scholar

18 B. C. Barnett, L. Rahman, M. N. Islam, Y. C. Chen, P. Bhattacharya, W. Riha, K. V. Reddy, A. T. Howe, K. A. Stair, H. Iwamura, S. R. Friberg, T. Mukai, *Opt. Lett.* 1995, **20**, 471.
Crossref | CAS | PubMed | Web of Science® | Google Scholar

19 O. Okhotnikov, T. Jouhti, J. Konttinen, S. Karirinne, M. Pessa, *Opt. Lett.* 2003, **28**, 364.
Crossref | CAS | PubMed | Web of Science® | Google Scholar

20 S. Set, H. Yaguchi, Y. Tanaka, M. Jablonski, Y. Sakakibara, A. Rozhin, M. Tokumoto, H. Kataura, Y. Achiba, K. Kikuchi, in *Optical Fiber Communication Conference*, Optical Society of America, Washington DC 2003, PD44.
Google Scholar

21 B. Fu, D. Popa, Z. Zhao, S. A. Hussain, E. Flahaut, T. Hasan, G. Soavi, A. C. Ferrari, *Appl. Phys. Lett.* 2018, **113**, 193102.
Crossref | Web of Science® | Google Scholar

22 Y. Song, S. Chen, Q. Zhang, L. Li, L. Zhao, H. Zhang, D. Tang, *Opt. Express* 2016, **24**, 25933.
Crossref | CAS | PubMed | Web of Science® | Google Scholar

23 J. Du, M. Zhang, Z. Guo, J. Chen, X. Zhu, G. Hu, P. Peng, Z. Zheng, H. Zhang, *Sci. Rep.* 2017, **7**, 42357.
Crossref | CAS | PubMed | Web of Science® | Google Scholar

24 W. Tao, X. Ji, X. Zhu, L. Li, J. Wang, Y. Zhang, P. E. Saw, W. Li, N. Kong, M. A. Islam, T. Gan, X. Zeng, H. Zhang, M. Mahmoudi, G. J. Tearney, Omid C Farokhzad, *Adv. Mater.* 2018, **30**, 1802061.
Wiley Online Library | PubMed | Web of Science® | Google Scholar

25 S. Yamashita, Y. Inoue, S. Maruyama, Y. Murakami, H. Yaguchi, M. Jablonski, S. Set, *Opt. Lett.* 2004, **29**, 1581.
Crossref | CAS | PubMed | Web of Science® | Google Scholar

26 Q. Bao, H. Zhang, Y. Wang, Z. Ni, Y. Yan, Z. X. Shen, K. P. Loh, D. Y. Tang, *Adv. Funct. Mater.* 2009,

Loading [MathJax]/jax/output/HTML-CSS/fonts/STIX-Web/Normal/Italic/Main.js

Wiley Online Library | CAS | Web of Science® | Google Scholar

27 B. Fu, Y. Hua, X. Xiao, H. Zhu, Z. Sun, C. Yang, *IEEE J. Sel. Top. Quantum Electron.* 2014, **20**, 411.
Crossref | CAS | Web of Science® | Google Scholar

28 Z.-X. Ding, Y. Chen, F. Xu, *Opt. Laser Technol.* 2021, **143**, 107381.
Crossref | CAS | Web of Science® | Google Scholar

29 B. Fu, J. Li, Z. Cao, D. Popa, *Photonics Res.* 2019, **7**, 116.
Crossref | CAS | Web of Science® | Google Scholar

30 F. Torrisi, D. Popa, S. Milana, Z. Jiang, T. Hasan, E. Lidorikis, A. C. Ferrari, *Adv. Opt. Mater.* 2016, **4**, 1088.
Wiley Online Library | CAS | Web of Science® | Google Scholar

31 B. Yao, S.-W. Huang, Y. Liu, A. K. Vinod, C. Choi, M. Hoff, Y. Li, M. Yu, Z. Feng, D.-L. Kwong, Y. Huang, Y. Rao, X. Duan, C. W. Wong, *Nature* 2018, **558**, 410.
Crossref | CAS | PubMed | Web of Science® | Google Scholar

32 T. Hasan, Z. Sun, F. Wang, F. Bonaccorso, P. H. Tan, A. G. Rozhin, A. C. Ferrari, *Adv. Mater.* 2009, **21**, 3874.
Wiley Online Library | CAS | Web of Science® | Google Scholar

33 C. Zhao, H. Zhang, X. Qi, Y. Chen, Z. Wang, S. Wen, D. Tang, *Appl. Phys. Lett.* 2012, **101**, 211106.
Crossref | CAS | Web of Science® | Google Scholar

34 S. Chen, L. Miao, X. Chen, Y. Chen, C. Zhao, S. Datta, Y. Li, Q. Bao, H. Zhang, Y. Liu, S. Wen, D. Fan, *Adv. Opt. Mater.* 2015, **3**, 1769.
Wiley Online Library | CAS | Web of Science® | Google Scholar

35 Q. Wang, Y. Chen, G. Jiang, L. Miao, C. Zhao, X. Fu, S. Wen, H. Zhang, *IEEE Photonics J.* 2015, **7**, 1500911.
Google Scholar

36 M. Liu, Z.-R. Cai, S. Hu, A.-P. Luo, C.-J. Zhao, H. Zhang, W.-C. Xu, Z.-C. Luo, *Opt. Lett.* 2015, **40**, 4767.
Crossref | CAS | PubMed | Web of Science® | Google Scholar

37 P. Yan, R. Lin, H. Chen, H. Zhang, A. Liu, H. Yang, S. Ruan, *IEEE Photonics Technol. Lett.* 2014, **27**, 264.
Web of Science® | Google Scholar

38 Y. Chen, C. Zhao, S. Chen, J. Du, P. Tang, G. Jiang, H. Zhang, S. Wen, D. Tang, *IEEE J. Sel. Top.*

Loading [MathJax]/jax/output/HTML-CSS/fonts/STIX-Web/Normal/Italic/Main.js

Crossref | Web of Science® | Google Scholar

39 H. Zhang, S. Lu, J.-l. Zheng, J. Du, S. Wen, D. Tang, K. Loh, *Opt. Express* 2014, **22**, 7249.
Crossref | CAS | PubMed | Web of Science® | Google Scholar

40 H. Yang, X. Li, Y. Wang, W. Jin, *Opt. Laser Technol.* 2021, **138**, 106924.
Crossref | CAS | Web of Science® | Google Scholar

41 P. G. Vianna, A. d. S. Almeida, R. M. Gerosa, D. A. Bahamon, C. J. de Matos, *Nanoscale Adv.* 2021, **3**, 272.
Crossref | CAS | Web of Science® | Google Scholar

42 M. Zhang, R. C. Howe, R. I. Woodward, E. J. Kelleher, F. Torrisi, G. Hu, S. V. Popov, J. R. Taylor, T. Hasan, *Nano Res.* 2015, **8**, 1522.
Crossref | CAS | Web of Science® | Google Scholar

43 W. Li, J. Peng, Y. Zhong, D. Wu, H. Lin, Y. Cheng, Z. Luo, J. Weng, H. Xu, Z. Cai, *Opt. Mater. Express* 2016, **6**, 2031.
Crossref | CAS | Web of Science® | Google Scholar

44 J. Lee, J. Koo, J. Lee, Y. M. Jhon, J. H. Lee, *Opt. Mater. Express* 2017, **7**, 2968.
Crossref | CAS | Web of Science® | Google Scholar

45 Z. Luo, Y. Huang, M. Zhong, Y. Li, J. Wu, B. Xu, H. Xu, Z. Cai, J. Peng, J. Weng, *J. Lightwave Technol.* 2014, **32**, 4077.
Crossref | CAS | Web of Science® | Google Scholar

46 Y. Chen, G. Jiang, S. Chen, Z. Guo, X. Yu, C. Zhao, H. Zhang, Q. Bao, S. Wen, D. Tang, D. Fan, *Opt. Express* 2015, **23**, 12823.
Crossref | CAS | PubMed | Web of Science® | Google Scholar

47 C. Ma, P. Yin, K. Khan, A. K. Tareen, R. Huang, J. Du, Y. Zhang, Z. Shi, R. Cao, S. Wei, X. Wang, Y. Ge, Y. Song, L. Gao, *Small* 2021, **17**, 2006891.
Wiley Online Library | CAS | Web of Science® | Google Scholar

48 J. Ma, S. Lu, Z. Guo, X. Xu, H. Zhang, D. Tang, D. Fan, *Opt. Express* 2015, **23**, 22643.
Crossref | PubMed | Web of Science® | Google Scholar

49 Z.-C. Luo, M. Liu, Z.-N. Guo, X.-F. Jiang, A.-P. Luo, C.-J. Zhao, X.-F. Yu, W.-C. Xu, H. Zhang, *Opt. Express* 2015, **23**, 20030.
Crossref | CAS | PubMed | Web of Science® | Google Scholar

Loading [MathJax]/jax/output/HTML-CSS/fonts/STIX-Web/Normal/Italic/Main.js

50 Z. Wang, Y. Xu, S. C. Dhanabalan, J. Sophia, C. Zhao, C. Xu, Y. Xiang, J. Li, H. Zhang, *IEEE Photonics J.* 2016, **8**, 1503310.
Google Scholar

51 Y. Xu, X.-F. Jiang, Y. Ge, Z. Guo, Z. Zeng, Q.-H. Xu, H. Zhang, X.-F. Yu, D. Fan, *J. Mater. Chem. C* 2017, **5**, 3007.
Crossref | CAS | Web of Science® | Google Scholar

52 Y. Cheng, W. Lyu, Z. Wang, H. Ouyang, A. Zhang, J. Sun, T. Yang, B. Fu, B. He, *Nanotechnology* 2021, **32**, 392003.
Crossref | CAS | Web of Science® | Google Scholar

53 Y. I. Jhon, J. Koo, B. Anasori, M. Seo, J. H. Lee, Y. Gogotsi, Y. M. Jhon, *Adv. Mater.* 2017, **29**, 1702496.
Wiley Online Library | CAS | Web of Science® | Google Scholar

54 J. Liu, X. Jiang, R. Zhang, Y. Zhang, L. Wu, W. Lu, J. Li, Y. Li, H. Zhang, *Adv. Funct. Mater.* 2019, **29**, 1807326.
Wiley Online Library | Web of Science® | Google Scholar

55 B. Fu, J. Sun, C. Wang, C. Shang, L. Xu, J. Li, H. Zhang, *Small* 2021, **17**, 2006054.
Wiley Online Library | CAS | Web of Science® | Google Scholar

56 M. Tuo, C. Xu, H. Mu, X. Bao, Y. Wang, S. Xiao, W. Ma, L. Li, D. Tang, H. Zhang, M. Premaratne, B. Sun, H. M. Cheng, S. Li, W. Ren, Q. Bao, *ACS Photonics* 2018, **5**, 1808.
Crossref | CAS | Web of Science® | Google Scholar

57 Y. Shi, N. Xu, Q. Wen, *J. Lightwave Technol.* 2020, **38**, 1975.
Crossref | CAS | Web of Science® | Google Scholar

58 A. Zhang, Z. Wang, H. Ouyang, W. Lyu, J. Sun, Y. Cheng, B. Fu, *Nanomaterials* 2021, **11**, 1778.
Crossref | CAS | PubMed | Web of Science® | Google Scholar

59 P. Yin, X. Xu, Z. Jiang, Y. Hai, *Opt. Commun.* 2017, **405**, 378.
Crossref | CAS | Web of Science® | Google Scholar

60 J. Lv, X. Xu, P. Yin, *Sol. Energy* 2019, **194**, 554.
Crossref | Web of Science® | Google Scholar

61 S. Gao, X. Xu, P. Yin, *Renew. Energy* 2020, **150**, 1178.
Crossref | Web of Science® | Google Scholar

Loading [MathJax]/jax/output/HTML-CSS/fonts/STIX-Web/Normal/Italic/Main.js

62 J. Lv, X. Xu, P. Yin, *J. Clean Prod.* 2020, **266**, 121895.
Crossref | Web of Science® | Google Scholar

63 Z. Sun, Y. Zhao, Z. Li, H. Cui, Y. Zhou, W. Li, W. Tao, H. Zhang, H. Wang, P. K. Chu, X.-F. Yu, *Small* 2017, **13**, 1602896.
Wiley Online Library | CAS | Web of Science® | Google Scholar

64 F. Yin, K. Hu, S. Chen, D. Wang, J. Zhang, M. Xie, D. Yang, M. Qiu, H. Zhang, Z.-g. Li, *J. Mater. Chem. B* 2017, **5**, 5433.
Crossref | CAS | PubMed | Web of Science® | Google Scholar

65 W. Liu, M. Liu, X. Liu, X. Wang, H.-X. Deng, M. Lei, Z. Wei, Z. Wei, *Adv. Opt. Mater.* 2020, **8**, 1901631.
Wiley Online Library | CAS | Web of Science® | Google Scholar

66 M. Zhang, Q. Wu, F. Zhang, L. Chen, X. Jin, Y. Hu, Z. Zheng, H. Zhang, *Adv. Opt. Mater.* 2019, **7**, 1800224.
Wiley Online Library | Web of Science® | Google Scholar

67 B. Fu, J. Sun, G. Wang, C. Shang, Y. Ma, J. Ma, L. Xu, V. Scardaci, *Nanophotonics* 2020, **9**, 2169.
Crossref | CAS | Web of Science® | Google Scholar

68 Z. Chu, J. Liu, Z. Guo, H. Zhang, *Opt. Mater. Express* 2016, **6**, 2374.
Crossref | CAS | Web of Science® | Google Scholar

69 J. Li, H. Luo, B. Zhai, R. Lu, Z. Guo, H. Zhang, Y. Liu, *Sci. Rep.* 2016, **6**, 30361.
Crossref | CAS | PubMed | Web of Science® | Google Scholar

70 J. Liu, J. Liu, Z. Guo, H. Zhang, W. Ma, J. Wang, L. Su, *Opt. Express* 2016, **24**, 30289.
Crossref | CAS | PubMed | Web of Science® | Google Scholar

71 J. Pei, J. Yang, T. Yildirim, H. Zhang, Y. Lu, *Adv. Mater.* 2019, **31**, 1706945.
Wiley Online Library | PubMed | Web of Science® | Google Scholar

72 J. He, L. Tao, H. Zhang, B. Zhou, J. Li, *Nanoscale* 2019, **11**, 2577.
Crossref | CAS | PubMed | Web of Science® | Google Scholar

73 A. K. Geim, K. S. Novoselov**2007**, *6*, 183.
Google Scholar

Loading [MathJax]/jax/output/HTML-CSS/fonts/STIX-Web/Normal/Italic/Main.js

ys. 2009, **5**, 438.
Crossref | CAS | Web of Science® | Google Scholar

75 S. Chen, C. Zhao, Y. Li, H. Huang, S. Lu, H. Zhang, S. Wen, *Opt. Mater. Express* 2014, **4**, 587.
Crossref | Web of Science® | Google Scholar

76 M. Chhowalla, H. S. Shin, G. Eda, L.-J. Li, K. P. Loh, H. Zhang, *Nat. Chem.* 2013, **5**, 263.
Crossref | PubMed | Web of Science® | Google Scholar

77 Q. H. Wang, K. Kalantar-Zadeh, A. Kis, J. N. Coleman, M. S. Strano, *Nat. Nanotechnol.* 2012, **7**, 699.
Crossref | CAS | PubMed | Web of Science® | Google Scholar

78 H. Liu, Y. Du, Y. Deng, D. Y. Peide, *Chem. Soc. Rev.* 2015, **44**, 2732.
Crossref | CAS | PubMed | Web of Science® | Google Scholar

79 Z. Qin, T. Hai, G. Xie, J. Ma, P. Yuan, L. Qian, L. Li, L. Zhao, D. Shen, *Opt. Express* 2018, **26**, 8224.
Crossref | CAS | PubMed | Web of Science® | Google Scholar

80 J. Halim, M. R. Lukatskaya, K. M. Cook, J. Lu, C. R. Smith, L.-Å. Näslund, S. J. May, L. Hultman, Y. Gogotsi, P. Eklund, M. W. Barsoum, *Chem. Mat.* 2014, **26**, 2374.
Crossref | CAS | PubMed | Web of Science® | Google Scholar

81 T. Jiang, Y. Xu, Q. Tian, L. Liu, Z. Kang, R. Yang, G. Qin, W. Qin, *Appl. Phys. Lett.* 2012, **101**, 151122.
Crossref | CAS | Web of Science® | Google Scholar

82 H. Guo, M. Feng, F. Song, H. Li, A. Ren, X. Wei, Y. Li, X. Xu, J. Tian, *IEEE Photonics Technol. Lett.* 2016, **28**, 135.
Crossref | CAS | Web of Science® | Google Scholar

83 D. Wu, H. Lin, Z. Cai, J. Peng, Y. Cheng, J. Weng, H. Xu, *IEEE Photonics J.* 2016, **8**, 4501507.
Google Scholar

84 X. Bai, C. Mou, L. Xu, S. Wang, S. Pu, X. Zeng, *Appl. Phys. Express* 2016, **9**, 042701.
Crossref | Web of Science® | Google Scholar

85 H. Ahmad, C. Lee, M. Ismail, Z. Ali, S. Reduan, N. Ruslan, M. Ismail, S. Harun, *Opt. Commun.* 2016, **381**, 72.
Crossref | CAS | Web of Science® | Google Scholar

86 H. Ahmad, S. A. Reduan, Z. A. Ali, M. Ismail, N. Ruslan, C. Lee, R. Puteh, S. W. Harun, *IEEE Photonics J.* 2015, **8**, 1500107.
Google Scholar

Loading [MathJax]/jax/output/HTML-CSS/fonts/STIX-Web/Normal/Italic/Main.js

87 M. Condorelli, V. Scardaci, M. Pulvirenti, L. D'Urso, F. Neri, G. Compagnini, E. Fazio, *Photonics* 2021, **8**, 299.
Crossref | CAS | Web of Science® | Google Scholar

88 W. Zhang, G. Feng, S. Dai, H. Zhang, Y. Ju, S. Ning, C. Yang, Y. Xiao, S. Zhou, *Laser Phys.* 2018, **28**, 095104.
Crossref | Web of Science® | Google Scholar

89 A. R. Muhammad, R. Zakaria, M. T. Ahmad, P. Wang, S. W. Harun, *Opt. Fiber Technol.* 2019, **50**, 23.
Crossref | CAS | Web of Science® | Google Scholar

90 D. Wu, J. Peng, Z. Cai, J. Weng, Z. Luo, N. Chen, H. Xu, *Opt. Express* 2015, **23**, 24071.
Crossref | CAS | PubMed | Web of Science® | Google Scholar

91 G. Jiang, Y. Jin, L. Miao, L. Du, Z. Kang, B. Huang, C. Zhao, S. Wen, *IEEE Photonics J.* 2017, **9**, 6102009.
Crossref | Web of Science® | Google Scholar

92 Z. Kang, X. Guo, Z. Jia, Y. Xu, L. Liu, D. Zhao, G. Qin, W. Qin, *Opt. Mater. Express* 2013, **3**, 1986.
Crossref | Web of Science® | Google Scholar

93 Z. Kang, M. Liu, X. Gao, N. Li, S. Yin, G. Qin, W. Qin, *Laser Phys. Lett.* 2015, **12**, 045105.
Crossref | Web of Science® | Google Scholar

94 Y. Shu, P. Guo, X. Li, G. Li, P. Wang, G. Shen, J. Li, *Front. Chem.* 2019, **7**, 715.
Crossref | CAS | PubMed | Web of Science® | Google Scholar

95 X.-D. Wang, Z.-C. Luo, H. Liu, M. Liu, A.-P. Luo, W.-C. Xu, *Appl. Phys. Lett.* 2014, **105**, 161107.
Crossref | CAS | Web of Science® | Google Scholar

96 H. Wu, J. Song, J. Wu, J. Xu, H. Xiao, J. Leng, P. Zhou, *IEEE J. Sel. Top. Quantum Electron.* 2017, **24**, 0901206.
Google Scholar

97 F. Zhang, H.-N. Zhang, D.-H. Liu, J. Liu, F.-K. Ma, D.-P. Jiang, S.-Y. Pang, L.-B. Su, J. Xu, *Chin. Phys. B* 2017, **26**, 024205.
Crossref | Web of Science® | Google Scholar

98 R. Li, C. Pang, Z. Li, N. Dong, J. Wang, F. Ren, S. Akhmadaliev, S. Zhou, F. Chen, *Nanophotonics* 2019, **8**, 859.
Crossref | CAS | Web of Science® | Google Scholar

Loading [MathJax]/jax/output/HTML-CSS/fonts/STIX-Web/Normal/Italic/Main.js

99 R. Z. R. R. Rosdin, M. T. Ahmad, A. R. Muhammad, Z. Jusoh, H. Arof, S. W. Harun, *Chin. Phys. Lett.* 2019, **36**, 054202.
Crossref | CAS | Web of Science® | Google Scholar

100 B. Fu, P. Wang, Y. Li, M. Condorelli, E. Fazio, J. Sun, L. Xu, V. Scardaci, G. Compagnini, *Nanophotonics* 2020, **9**, 3873.
Crossref | CAS | Web of Science® | Google Scholar

101 B. Fu, C. Zhang, P. Wang, M. Condorelli, M. Pulvirenti, E. Fazio, C. Shang, J. Li, Y. Li, G. Compagnini, V. Scardaci, *J. Lightwave Technol.* 2021, **39**, 2084.
Crossref | CAS | Web of Science® | Google Scholar

102 E. I. Ismail, F. Ahmad, S. Ambran, A. A. Latiff, S. W. Harun, in *AIP Conference Proceedings*, Vol. **2203**, AIP Publishing LLC, Melville, NY 2020, p. 020004.
Google Scholar

103 E. Ismail, F. Ahmad, S. Shafie, H. Yahaya, A. Latif, F. Muhammad, *Results Phys.* 2020, **18**, 103228.
Crossref | Web of Science® | Google Scholar

104 A. Muhammad, M. Ahmad, R. Zakaria, H. Rahim, S. Yusoff, K. Hamdan, H. Yusof, H. Arof, S. Harun, *Chin. Phys. Lett.* 2017, **34**, 034205.
Crossref | Web of Science® | Google Scholar

105 C. Pang, R. Li, Z. Li, N. Dong, H. Amekura, S. Wang, H. Yu, J. Wang, F. Ren, N. Ishikawa, N. Okubo, F. Chen, *ACS Appl. Mater. Inter.* 2019, **2**, 5871.
Crossref | CAS | Web of Science® | Google Scholar

106 S. Wang, C. Pang, Z. Li, R. Li, N. Dong, Q. Lu, F. Ren, J. Wang, F. Chen, *Opt. Mater. Express* 2019, **9**, 3808.
Crossref | CAS | Web of Science® | Google Scholar

107 L. Li, R. Lv, S. Liu, Z. Chen, J. Wang, Y. Wang, W. Ren, W. Liu, *Opt. Mater. Express* 2019, **9**, 731.
Crossref | CAS | Web of Science® | Google Scholar

108 N. Li, H. Jia, J. Liu, L. Cui, Z. Jia, Z. Kang, G. Qin, W. Qin, *Laser Phys. Lett.* 2019, **16**, 065102.
Crossref | CAS | Web of Science® | Google Scholar

109 C. Ma, J. Peng, X. Yang, H. Zhang, Q. Zhao, D. Li, X. Su, Y. Zheng, *Opt. Commun.* 2020, **473**, 125979.
Crossref | CAS | Web of Science® | Google Scholar

Loading [MathJax]/jax/output/HTML-CSS/fonts/STIX-Web/Normal/Italic/Main.js

110 D. Mao, X. Cui, Z. He, H. Lu, W. Zhang, L. Wang, Q. Zhuang, S. Hua, T. Mei, J. Zhao, *Nanoscale* 2018, **10**, 21219.
Crossref | CAS | PubMed | Web of Science® | Google Scholar

111 H. Ahmad, M. Z. Samion, A. Kamely, M. F. Ismail, *Infrared Phys. Technol.* 2019, **97**, 142.
Crossref | CAS | Web of Science® | Google Scholar

112 A. H. H. Al-Masoodi, M. H. M. Ahmed, A. A. Latiff, H. Arof, S. W. Harun, *J. Mod. Opt.* 2018, **65**, 1801.
Crossref | CAS | Web of Science® | Google Scholar

113 A. Nady, M. H. M. Ahmed, A. A. Latiff, A. Numan, C. R. Ooi, S. W. Harun, *Laser Phys.* 2017, **27**, 065105.
Crossref | Web of Science® | Google Scholar

114 A. H. Al-Masoodi, O. B. Abdulghafoor, I. Alani, M. Ahmed, A. H. Al Masoodi, S. Harun, *Opt. Mater. Express* 2020, **10**, 2896.
Crossref | CAS | Web of Science® | Google Scholar

115 S. A. Sadeq, S. W. Harun, A. H. Al-Janabi, *Appl. Optics* 2018, **57**, 5180.
Crossref | CAS | PubMed | Web of Science® | Google Scholar

116 M. F. M. Rusdi, A. A. Latiff, M. C. Paul, S. Das, A. Dhar, H. Ahmad, S. W. Harun, *Opt. Laser Technol.* 2017, **89**, 16.
Crossref | Web of Science® | Google Scholar

117 N. M. Yusoff, C. Abdullah, M. A. Hadi, E. Ng, H. Lee, N. Z. Abidin, N. Rosli, M. Mahdi, *Optik* 2020, **218**, 164998.
Crossref | Web of Science® | Google Scholar

118 A. Nady, M. F. Baharom, A. A. Latiff, S. W. Harun, *Chin. Phys. Lett.* 2018, **35**, 044204.
Crossref | Web of Science® | Google Scholar

119 A. Nady, A. A. Latiff, A. Numan, C. R. Ooi, S. W. Harun, *Laser Phys.* 2018, **28**, 085106.
Crossref | Web of Science® | Google Scholar

120 Z. Rizman, N. Zulkipli, S. Adwan, H. Arof, R. Apsari, S. Harun, *Indian J. Phys*. DOI: 10.1007/s12648–020–01974–2.
Google Scholar

121 J. Guo, H. Zhang, C. Zhang, Z. Li, Y. Sheng, C. Li, X. Bao, B. Man, Y. Jiao, S. Jiang, *Opt. Mater. Express*

Loading [MathJax]/jax/output/HTML-CSS/fonts/STIX-Web/Normal/Italic/Main.js

Crossref | CAS | Web of Science® | Google Scholar

122 J. Guo, H. Zhang, Z. Li, Y. Sheng, Q. Guo, X. Han, Y. Liu, B. Man, T. Ning, S. Jiang, *Opt. Mater.* 2018, **78**, 432.
Crossref | CAS | Web of Science® | Google Scholar

123 B. Nizamani, A. A. A. Jafry, M. A. Khudus, F. A. Memon, A. Shuhaimi, N. Kasim, E. Hanafi, M. Yasin, S. W. Harun, *Opt. Laser Technol.* 2020, **124**, 105998.
Crossref | CAS | Web of Science® | Google Scholar

124 B. Nizamani, S. Salam, A. Jafry, N. Zahir, N. Jurami, M. A. Khudus, A. Shuhaimi, E. Hanafi, S. Harun, *Chin. Phys. Lett.* 2020, **37**, 054202.
Crossref | CAS | Web of Science® | Google Scholar

125 B. Nizamani, A. Jafry, M. A. Khudus, A. Rosol, F. Samsamnun, N. Kasim, E. Hanafi, A. Shuhaimi, S. Harun, *Opt. Fiber Technol.* 2020, **55**, 102124.
Crossref | CAS | Web of Science® | Google Scholar

126 W. Niu, L. Zhang, G. Xu, *Nanoscale* 2013, **5**, 3172.
Crossref | CAS | PubMed | Web of Science® | Google Scholar

127 B. Nikoobakht, M. A. El-Sayed, *Chem. Mat.* 2003, **15**, 1957.
Crossref | CAS | Web of Science® | Google Scholar

128 X. Ye, L. Jin, H. Caglayan, J. Chen, G. Xing, C. Zheng, V. Doan-Nguyen, Y. Kang, N. Engheta, C. R. Kagan, C. B. Murray, *ACS Nano* 2012, **6**, 2804.
Crossref | CAS | PubMed | Web of Science® | Google Scholar

129 H.-Y. Wu, H.-C. Chu, T.-J. Kuo, C.-L. Kuo, M. H. Huang, *Chem. Mat.* 2005, **17**, 6447.
Crossref | CAS | Web of Science® | Google Scholar

130 X. Wang, Z. Luo, M. Liu, R. Tang, A. Luo, W. Xu, *Laser Phys. Lett.* 2016, **13**, 045101.
Crossref | Web of Science® | Google Scholar

131 G. Compagnini, M. Condorelli, M. E. Fragalà, V. Scardaci, I. Tinnirello, O. Puglisi, F. Neri, E. Fazio, *J. Nanomater.* 2019, **2019**.
Crossref | Web of Science® | Google Scholar

132 D. Wu, H. Lin, Z. Cai, J. Peng, Y. Cheng, J. Weng, H. Xu, *IEEE Photonics J.* 2016, **8**, 4501507.
Google Scholar

Loading [MathJax]/jax/output/HTML-CSS/fonts/STIX-Web/Normal/Italic/Main.js

133 P. J. P. Espitia, N. d. F. F. Soares, J. S. dos Reis Coimbra, N. J. de Andrade, R. S. Cruz, E. A. A. Medeiros, *Food Bioprocess. Technol.* 2012, **5**, 1447.
Crossref | CAS | Web of Science® | Google Scholar

134 L.-E. Shi, Z.-H. Li, W. Zheng, Y.-F. Zhao, Y.-F. Jin, Z.-X. Tang, *Food Addit. Contam., Part A* 2014, **31**, 173.
Crossref | CAS | Web of Science® | Google Scholar

135 A. Naveed Ul Haq, A. Nadhman, I. Ullah, G. Mustafa, M. Yasinzai, I. Khan, *J. Nanomater.* 2017, **2017**, 8510342.
Crossref | Web of Science® | Google Scholar

136 S. Gharpure, B. Ankamwar, *J. Nanosci. Nanotechnol.* 2020, **20**, 5977.
Crossref | CAS | PubMed | Web of Science® | Google Scholar

137 N. S. Rosli, C. A. C. Abdullah, R. Hazan, *Results Phys.* 2018, **11**, 72.
Crossref | Web of Science® | Google Scholar

138 R. Jin, Y. Cao, C. A. Mirkin, K. L. Kelly, G. C. Schatz, J. Zheng, *Science* 2001, **294**, 1901.
Crossref | CAS | PubMed | Web of Science® | Google Scholar

139 G. R. Rao, H. R. Sahu, *J. Chem. Sci.* 2001, **113**, 651.
Crossref | CAS | Google Scholar

140 M. Humayun, A. Zada, Z. Li, M. Xie, X. Zhang, Y. Qu, F. Raziq, L. Jing, *Appl. Catal. B-Environ.* 2016, **180**, 219.
Crossref | CAS | Web of Science® | Google Scholar

141 X. Li, Z. Zhang, F.-J. Zhang, J. Liu, J. Ye, W.-C. Oh, *J. Korean Ceram. Soc.* 2016, **53**, 665.
Crossref | CAS | Web of Science® | Google Scholar

142 A. Manikandan, J. J. Vijaya, J. A. Mary, L. J. Kennedy, A. Dinesh, *J. Ind. Eng. Chem.* 2014, **20**, 2077.
Crossref | CAS | Web of Science® | Google Scholar

143 A. Radoń, A. Drygała, Ł. Hawełek, D. Łukowiec, *Mater. Charact.* 2017, **131**, 148.
Crossref | CAS | Web of Science® | Google Scholar

144 H. M. Fan, G. J. You, Y. Li, Z. Zheng, H. R. Tan, Z. X. Shen, S. H. Tang, Y. P. Feng, *J. Phys. Chem. C* 2009, **113**, 9928.
Crossref | CAS | Web of Science® | Google Scholar

Loading [MathJax]/jax/output/HTML-CSS/fonts/STIX-Web/Normal/Italic/Main.js

145 X. Wang, Y. Wang, D. Mao, L. Li, Z. Chen, *Opt. Mater. Express* 2017, **7**, 2913.
Crossref | CAS | Web of Science® | Google Scholar

146 G. Chatzikyriakos, K. Iliopoulos, A. Bakandritsos, S. Couris, *Chem. Phys. Lett.* 2010, **493**, 314.
Crossref | CAS | Web of Science® | Google Scholar

147 M. Kahouli, A. Barhoumi, A. Bouzid, A. Al-Hajry, S. Guermazi, *Superlattices Microstruct.* 2015, **85**, 7.
Crossref | CAS | Web of Science® | Google Scholar

148 C. Klingshirn, *Chemphyschem* 2007, **8**, 782.
Wiley Online Library | CAS | PubMed | Web of Science® | Google Scholar

149 N. Satoh, T. Nakashima, K. Kamikura, K. Yamamoto, *Nat. Nanotechnol.* 2008, **3**, 106.
Crossref | CAS | PubMed | Web of Science® | Google Scholar

150 V. N. Kuznetsov, N. Serpone, *J. Phys. Chem. B* 2006, **110**, 25203.
Crossref | CAS | PubMed | Web of Science® | Google Scholar

151 J.-H. Lin, Y.-J. Chen, H.-Y. Lin, W.-F. Hsieh, *J. Appl. Phys.* 2005, **97**, 033526.
Crossref | CAS | Web of Science® | Google Scholar

152 M. Shahmiri, N. A. Ibrahim, N. Faraji, W. M. M. Yunus, N. Asim, N. Zainuddin, *Physica E: Low-dimens. Syst. Nanostruct.* 2013, **54**, 109.
Crossref | CAS | Web of Science® | Google Scholar

153 R. W. Boyd, *Nonlinear Optics*, 3rd ed., Academic Press, Inc., San Diego, CA 2008.
Crossref | Google Scholar

154 M. Sheik-Bahae, A. Said, T.-H. Wei, D. Hagan, E. Van Stryland, *IEEE J. Quantum Electron.* 1990, **26**, 760.
Crossref | CAS | Web of Science® | Google Scholar

155 A. Martinez, Z. Sun, *Nat. Photonics* 2013, **7**, 842.
Crossref | CAS | Web of Science® | Google Scholar

156 M. Hajlaoui, E. Papalazarou, J. Mauchain, G. Lantz, N. Moisan, D. Boschetto, Z. Jiang, I. Miotkowski, Y. Chen, A. Taleb-Ibrahimi, et al., *Nano Lett.* 2012, **12**, 3532.
Crossref | CAS | PubMed | Web of Science® | Google Scholar

Loading [MathJax]/jax/output/HTML-CSS/fonts/STIX-Web/Normal/Italic/Main.js

Peng, X. Liu, et al., *Sci. Rep.* 2013, **3**, 2411.

Crossref | PubMed | Web of Science® | Google Scholar

158 J. O. Island, G. A. Steele, H. S. van der Zant, A. Castellanos-Gomez, *2D Mater.* 2015, **2**, 011002.
Crossref | Web of Science® | Google Scholar

159 R. Ghosh Chaudhuri, S. Paria, *Chem. Rev.* 2012, **112**, 2373.
Crossref | CAS | PubMed | Web of Science® | Google Scholar

160 P. C. Ray, *Chem. Rev.* 2010, **110**, 5332.
Crossref | CAS | PubMed | Web of Science® | Google Scholar

161 Y. Zhang, X. Hu, H. Yang, Q. Gong, *Appl. Phys. Lett.* 2011, **99**, 141113.
Crossref | CAS | Web of Science® | Google Scholar

162 H. Liao, R. Xiao, J. Fu, P. Yu, G. K. L. Wong, P. Sheng, *Appl. Phys. Lett.* 1997, **70**, 1.
Crossref | CAS | Web of Science® | Google Scholar

163 K.-H. Kim, A. Husakou, J. Herrmann, *Opt. Express* 2010, **18**, 21918.
Crossref | CAS | PubMed | Web of Science® | Google Scholar

164 R. Philip, G. R. Kumar, N. Sandhyarani, T. Pradeep, *Phys. Rev. B* 2000, **62**, 13160.
Crossref | CAS | Web of Science® | Google Scholar

165 P. K. Jain, X. Huang, I. H. El-Sayed, M. A. El-Sayed, *Plasmonics* 2007, **2**, 107.
Crossref | CAS | Web of Science® | Google Scholar

166 H. Baida, D. Mongin, D. Christofilos, G. Bachelier, A. Crut, P. Maioli, N. Del Fatti, F. Vallée, *Phys. Rev. Lett.* 2011, **107**, 057402.
Crossref | CAS | PubMed | Web of Science® | Google Scholar

167 M. A. El-Sayed, *Accounts Chem. Res.* 2001, **34**, 257.
Crossref | CAS | PubMed | Web of Science® | Google Scholar

168 C. J. Murphy, T. K. Sau, A. M. Gole, C. J. Orendorff, J. Gao, L. Gou, S. E. Hunyadi, T. Li, *J. Phys. Chem. B* 2005, **109**, 13857.
Crossref | CAS | PubMed | Web of Science® | Google Scholar

169 W. S. Choi, M. F. Chisholm, D. J. Singh, T. Choi, G. E. Jellison, H. N. Lee, *Nat. Commun.* 2012, **3**, 689.
Crossref | CAS | PubMed | Web of Science® | Google Scholar

Loading [MathJax]/jax/output/HTML-CSS/fonts/STIX-Web/Normal/Italic/Main.js

170 M. Ando, K. Kadono, M. Haruta, T. Sakaguchi, M. Miya, *Nature* 1995, **374**, 625.

Crossref | CAS | Web of Science® | Google Scholar

171 Z. L. Wang, *J. Phys. Condens. Matter* 2004, **16**, R829.
Crossref | CAS | Web of Science® | Google Scholar

172 Y. Tsutsui, T. Hayakawa, G. Kawamura, M. Nogami, *Nanotechnology* 2011, **22**, 275203.
Crossref | PubMed | Web of Science® | Google Scholar

173 K.-H. Kim, U. Griebner, J. Herrmann, *Opt. Express* 2012, **20**, 16174.
Crossref | CAS | Web of Science® | Google Scholar

174 Y. H. Lee, Y. Yan, L. Polavarapu, Q.-H. Xu, *Appl. Phys. Lett.* 2009, **95**, 023105.
Crossref | CAS | Web of Science® | Google Scholar

175 H. Ahmad, R. A. A. Tahrin, N. Azman, S. Kassim, M. A. Ismail, M. J. Maah, *Opt. Commun.* 2017, **403**, 115.
Crossref | CAS | Web of Science® | Google Scholar

176 A. H. A. Rosol, A. A. Latiff, M. I. M. A. Khudus, S. W. Harun, *Indian J. Phys.* 2020, **94**, 1079.
Crossref | CAS | Web of Science® | Google Scholar

177 X. Ye, L. Jin, H. Caglayan, J. Chen, G. Xing, C. Zheng, V. Doan-Nguyen, Y. Kang, N. Engheta, C. R. Kagan, et al., *ACS Nano* 2012, **6**, 2804.
Crossref | CAS | PubMed | Web of Science® | Google Scholar

178 H. I. Elim, J. Yang, J.-Y. Lee, J. Mi, W. Ji, *Appl. Phys. Lett.* 2006, **88**, 083107.
Crossref | CAS | Web of Science® | Google Scholar

179 H. Chen, L. Shao, Q. Li, J. Wang, *Chem. Soc. Rev.* 2013, **42**, 2679.
Crossref | CAS | PubMed | Web of Science® | Google Scholar

180 Z. Kang, Y. Xu, L. Zhang, Z. Jia, L. Liu, D. Zhao, Y. Feng, G. Qin, W. Qin, *Appl. Phys. Lett.* 2013, **103**, 041105.
Crossref | CAS | Web of Science® | Google Scholar

181 Z. Kang, Q. Li, X. J. Gao, L. Zhang, Z. X. Jia, Y. Feng, G. S. Qin, W. P. Qin, *Laser Phys. Lett.* 2014, **11**, 035102.
Crossref | CAS | Web of Science® | Google Scholar

182 X.-D. Wang, Q.-M. Liang, A.-P. Luo, Z.-C. Luo, M. Liu, Y.-F. Zhu, J.-P. Xue, S.-W. Li, *Opt. Eng.* 2019, **58**,
CAS | Google Scholar

Loading [MathJax]/jax/output/HTML-CSS/fonts/STIX-Web/Normal/Italic/Main.js

183 X. Wang, S. Yang, M. Sun, Q. Liang, S. Li, A. Luo, M. Liu, Z. Luo, *Laser Phys.* 2020, **30**, 065104.
Crossref | CAS | Web of Science® | Google Scholar

184 J. Lee, J. Koo, J. Lee, J. H. Lee, *J. Lightwave Technol.* 2016, **34**, 5250.
Crossref | CAS | Web of Science® | Google Scholar

185 J. Lee, J. Koo, J. H. Lee, *Laser Phys. Lett.* 2017, **14**, 090001.
Crossref | Web of Science® | Google Scholar

186 S. Lu, L. Du, Z. Kang, J. Li, B. Huang, G. Jiang, L. Miao, G. Qin, C. Zhao, S. Wen, *IEEE Photonics J.* 2018, **10**, 6101008.
CAS | Google Scholar

187 Z. Kang, M. Liu, C. Tang, X. Xu, Z. Jia, G. Qin, W. Qin, *Opt. Mater. Express* 2018, **8**, 3841.
Crossref | CAS | Web of Science® | Google Scholar

188 L. Cui, J. Liu, N. Li, F. Wang, Z. Jia, Z. Kang, W. Qin, G. Qin, *Laser Phys. Lett.* 2020, **17**, 115104.
Crossref | CAS | Web of Science® | Google Scholar

189 H. Luo, S. Li, X. Wu, Z. Kang, J. Li, G. Qin, W. Qin, Y. Liu, *Opt. Lett.* 2021, **46**, 1562.
Crossref | PubMed | Web of Science® | Google Scholar

190 F. Chen, J. Cheng, S. Dai, Z. Xu, W. Ji, R. Tan, Q. Zhang, *Opt. Express* 2014, **22**, 13438.
Crossref | CAS | PubMed | Web of Science® | Google Scholar

191 V. Singh, P. Aghamkar, *Appl. Phys. Lett.* 2014, **104**, 111112.
Crossref | CAS | Web of Science® | Google Scholar

192 Y. A. Krutyakov, A. A. Kudrinskiy, A. Y. Olenin, G. V. Lisichkin, *Russ. Chem. Rev.* 2008, **77**, 233.
Crossref | CAS | Google Scholar

193 D. A. Glubokov, V. V. Sychev, A. S. Mikhailov, A. E. Korolkov, D. A. Chubich, B. I. Shapiro, A. G. Vitukhnovskii, *Quantum Electron.* 2014, **44**, 314.
Crossref | Web of Science® | Google Scholar

194 Y. Qi, Y. Zhou, L. Wu, F. Yang, S. Peng, S. Zheng, D. Yin, *J. Lumin.* 2014, **153**, 401.
Crossref | CAS | Web of Science® | Google Scholar

195 H. Ahmad, M. Z. Samion, A. Muhamad, A. S. Sharbirin, M. F. Ismail, *Laser Phys. Lett.* 2016, **13**,
Crossref | Web of Science® | Google Scholar

Loading [MathJax]/jax/output/HTML-CSS/fonts/STIX-Web/Normal/Italic/Main.js

196 M. Ahmad, A. Muhammad, R. Zakaria, H. Ahmad, S. Harun, *Optik* 2020, **207**, 164455.
Crossref | CAS | Web of Science® | Google Scholar

197 A. Muhammad, A. Markom, S. Harun, Z. Jusoh, P. Yupapin, *Opt. Laser Technol.* 2021, **136**, 106791.
Crossref | CAS | Web of Science® | Google Scholar

198 H. H. Huang, F. Q. Yan, Y. M. Kek, C. H. Chew, G. Q. Xu, W. Ji, P. S. Oh, S. H. Tang, *Langmuir* 1997, **13**, 172.
Crossref | CAS | Web of Science® | Google Scholar

199 A. R. Muhammad, M.Yasin, M. T. Ahmad, M. Zakaria, H. R. A. Rahim, Z. Jusoh, H. Arof, S. W. Harun, *Dig. J. Nanomater. Biostruct.* 2018, **13**, 279.
Web of Science® | Google Scholar

200 A. R. Muhammad, M. T. Ahmad, R. Zakaria, P. P. Yupapin, S. W. Harun, M. Yasin, *J. Mod. Opt.* 2019, **66**, 1381.
Crossref | CAS | Web of Science® | Google Scholar

201 E. I. Ismail, F. Ahmad, S. Ambran, A. A. Latiff, S. W. Harun, *J. Phys.: Conf. Ser.* 2019, **1371**, 012028.
Crossref | CAS | Google Scholar

202 C. Ataca, H. Şahin, S. Ciraci, *J. Phys. Chem. C* 2012, **116**, 8983.
Crossref | CAS | Web of Science® | Google Scholar

203 D. Mao, X. Cui, W. Zhang, M. Li, T. Feng, B. Du, H. Lu, J. Zhao, *Photonics Res.* 2017, **5**, 52.
Crossref | CAS | Web of Science® | Google Scholar

204 T. Hashimoto, T. Yamada, T. Yoko, *J. Appl. Phys.* 1996, **80**, 3184.
Crossref | CAS | Web of Science® | Google Scholar

205 Y. Chen, J. Yin, H. Chen, J. Wang, P. Yan, S. Ruan, *IEEE Photonics J.* 2017, **9**, 1501009.
Google Scholar

206 J. Koo, J. Lee, J. Kim, J. H. Lee, *J. Lumin.* 2018, **195**, 181.
Crossref | CAS | Web of Science® | Google Scholar

207 X. Liu, K. Yang, S. Zhao, J. Zhao, T. Li, W. Qiao, G. Li, D. Li, B. Zhang, J. He, J. Bian, L. Zheng, L. Su, J. Xu, *IEEE Photonics Technol. Lett.* 2018, **30**, 777.
Crossref | Web of Science® | Google Scholar

Loading [MathJax]/jax/output/HTML-CSS/fonts/STIX-Web/Normal/Italic/Main.js

208 S. K. M. Al-Hayali, A. H. Al-Janabi, *Laser Phys.* 2018, **28**, 035103.

Crossref | Web of Science® | Google Scholar

209 L. Li, Y. Wang, X. Wang, R. Lv, S. Liu, Z. Chen, J. Wang, *Opt. Laser Technol.* 2018, **103**, 354.
Crossref | CAS | Web of Science® | Google Scholar

210 H. Wang, F. Zhao, Z. Yan, X. Hu, K. Zhou, T. Zhang, W. Zhang, Y. Wang, W. Zhao, L. Zhang, C. Sun, *Opt. Express* 2019, **27**, 15693.
Crossref | CAS | PubMed | Web of Science® | Google Scholar

211 J. Yang, J. Hu, H. Luo, J. Li, J. Liu, X. Li, Y. Liu, *Photonics Res.* 2020, **8**, 70.
Crossref | CAS | Web of Science® | Google Scholar

212 G. Chen, Y. Yang, M. Tian, C. Li, Y. Huang, M. Lv, *Opt. Mater. Express* 2020, **10**, 588.
Crossref | CAS | Web of Science® | Google Scholar

213 P. Cheng, Y. Du, M. Han, X. Shu, *Opt. Express* 2020, **28**, 13177.
Crossref | CAS | PubMed | Web of Science® | Google Scholar

214 N. Li, H. Jia, M. Guo, J. Zhang, W. Zhang, Z. Guo, M. Li, Z. Jia, G. Qin, *Opt. Fiber Technol.* 2021, **61**, 102421.
Crossref | CAS | Web of Science® | Google Scholar

215 U. Özgür, Y. I. Alivov, C. Liu, A. Teke, M. A. Reshchikov, S. Doğan, V. Avrutin, S.-J. Cho, H. Morkoç, *J. Appl. Phys.* 2005, **98**, 041301.
Crossref | CAS | Web of Science® | Google Scholar

216 C. Soci, A. Zhang, B. Xiang, S. A. Dayeh, D. P. R. Aplin, J. Park, X. Y. Bao, Y. H. Lo, D. Wang, *Nano Lett.* 2007, **7**, 1003.
Crossref | CAS | PubMed | Web of Science® | Google Scholar

217 J. C. Johnson, K. P. Knutsen, H. Yan, M. Law, Y. Zhang, P. Yang, R. J. Saykally, *Nano Lett.* 2004, **4**, 197.
Crossref | CAS | Web of Science® | Google Scholar

218 H. Ahmad, M. A. M. Salim, M. F. Ismail, S. W. Harun, *Laser Phys.* 2016, **26**, 115107.
Crossref | Web of Science® | Google Scholar

219 N. A. Aziz, A. A. Latiff, M. Q. Lokman, E. Hanafi, S. W. Harun, *Chin. Phys. Lett.* 2017, **34**, 044202.
Crossref | Web of Science® | Google Scholar

Loading [MathJax]/jax/output/HTML-CSS/fonts/STIX-Web/Normal/Italic/Main.js

oodi, A. A. Latiff, S. W. Harun, *Laser Phys.* 2018, **28**, 075105.

Crossref | Web of Science® | Google Scholar

221 S. A. S. Husin, F. D. Muhammad, C. A. C. Abdullah, S. H. Ribut, M. Z. Zulkifli, M. A. Mahdi, *Chin. Phys. B* 2019, **28**, 084207.
Crossref | CAS | Web of Science® | Google Scholar

222 F. Muhammad, S. Husin, E. Ng, K. Lau, C. Abdullah, M. Mahdi, *Chin. Phys. B* 2021, **30**, 054204.
Crossref | CAS | Web of Science® | Google Scholar

223 K. Iliopoulos, G. Kalogerakis, D. Vernardou, N. Katsarakis, E. Koudoumas, S. Couris, *Thin Solid Films* 2009, **518**, 1174.
Crossref | CAS | Web of Science® | Google Scholar

224 Z. Zhang, H. Wu, *Chem. Commun.* 2014, **50**, 14179.
Crossref | CAS | PubMed | Web of Science® | Google Scholar

225 H. Tang, K. Prasad, R. Sanjinès, P. E. Schmid, F. Lévy, *J. Appl. Phys.* 1994, **75**, 2042.
Crossref | CAS | Web of Science® | Google Scholar

226 J. T. Luxon, R. Summitt, *J. Chem. Phys.* 1969, **50**, 1366.
Crossref | CAS | Web of Science® | Google Scholar

227 H. Ahmad, M. A. M. Salim, Z. A. Ali, M. F. Ismail, K. Thambiratnam, A. A. Latif, N. Nayan, S. W. Harun, *Chin. Opt. Lett.* 2016, **14**, 091403.
Crossref | Web of Science® | Google Scholar

228 H. Ahmad, M. A. M. Salim, *IEEE J. Quantum Electron.* 2017, **53**, 1600306.
Google Scholar

229 P. H. Reddy, M. Rahman, M. Paul, A. Latiff, A. Rosol, S. Das, A. Dhar, S. K. Bhadra, K. Dimyati, S. Harun, *Optik* 2018, **158**, 1327.
Crossref | CAS | Web of Science® | Google Scholar

230 M. F. A. Rahman, P. H. Reddy, M. C. Paul, S. Das, A. Dhar, M. F. Baharom, A. A. Latiff, M. F. M. Rusdi, P. Wang, K. Dimyati, S. W. Harun, *Appl. Optics* 2019, **58**, 3495.
Crossref | CAS | PubMed | Web of Science® | Google Scholar

231 M. F. A. Rahman, P. H. Reddy, M. C. Paul, S. Das, A. Dhar, M. F. M. Rusdi, A. A. Latiff, K. Dimyati, S. W. Harun, *J. Phys.: Conf. Ser.* 2019, **1371**, 012023.
Crossref | CAS | Google Scholar

Loading [MathJax]/jax/output/HTML-CSS/fonts/STIX-Web/Normal/Italic/Main.js

232 X. Wang, Y. Wang, Y. Gu, L. Li, J. Wang, X. Yang, Z. Chen, *IEEE Photonics J.* 2019, **11**, 1501110.

CAS | Google Scholar

233 R. P. de Melo, B. J. P. da Silva, F. E. P. dos Santos, A. Azevedo, C. B. de Araújo, *J. Appl. Phys.* 2009, **106**, 093517.
Crossref | Web of Science® | Google Scholar

234 S. W. Harun, B. M. Nawi, A. A. Latiff, *J. Nonlinear Opt. Phys. Mater.* 2018, **27**, 1850020.
Crossref | CAS | Web of Science® | Google Scholar

235 M. Rusdi, A. Rosol, M. Rahman, M. Mahyuddin, A. Latiff, H. Ahmad, S. Harun, M. Yasin, *Opt. Commun.* 2019, **447**, 6.
Crossref | CAS | Web of Science® | Google Scholar

236 G. S. Boltaev, R. A. Ganeev, P. S. Krishnendu, K. Zhang, C. Guo, *Sci. Rep.* 2019, **9**, 11414.
Crossref | PubMed | Web of Science® | Google Scholar

237 J. Jun, C. Jin, H. Kim, S. Park, C. Lee, *Appl. Surf. Sci.* 2009, **255**, 8544.
Crossref | CAS | Web of Science® | Google Scholar

238 S. A. Sadeq, S. K. Al-Hayali, S. W. Harun, A. Al-Janabi, *Results Phys.* 2018, **10**, 264.
Crossref | Web of Science® | Google Scholar

239 B. Yan, L. Liao, Y. You, X. Xu, Z. Zheng, Z. Shen, J. Ma, L. Tong, T. Yu, *Adv. Mater.* 2009, **21**, 2436.
Wiley Online Library | CAS | Web of Science® | Google Scholar

240 M. Molli, A. B. Kademane, P. Pradhan, V. S. Muthukumar, *Appl. Phys. A* 2016, **122**, 757.
Crossref | Web of Science® | Google Scholar

241 M. F. A. Rahman, M. F. M. Rusdi, S. W. Harun, M. Yasin, *Nonlinear Opt., Quantum Opt.* 2018, **48**, 295.
CAS | Web of Science® | Google Scholar

242 M. Z. Alam, I. D. Leon, R. W. Boyd, *Science* 2016, **352**, 795.
Crossref | CAS | PubMed | Web of Science® | Google Scholar

243 G. V. Naik, V. M. Shalaev, A. Boltasseva, *Adv. Mater.* 2013, **25**, 3264.
Wiley Online Library | CAS | PubMed | Web of Science® | Google Scholar

244 M. Kanehara, H. Koike, T. Yoshinaga, T. Teranishi, *J. Am. Chem. Soc.* 2009, **131**, 17736.
Crossref | CAS | PubMed | Web of Science® | Google Scholar

Loading [MathJax]/jax/output/HTML-CSS/fonts/STIX-Web/Normal/Italic/Main.js

245 M. A. Farag, M. El-Okr, R. M. Mahani, G. M. Turky, H. H. Afify, *Int. J. Adv. Eng., Technol. Comput. Sci.* 2014, **1**, 1.
Google Scholar

246 P. Płóciennik, D. Guichaoua, A. Zawadzka, A. Korcala, J. Strzelecki, P. Trzaska, B. Sahraoui, *Opt. Quantum Electron.* 2016, **48**.
Crossref | Web of Science® | Google Scholar

247 W. A. Khaleel, S. A. Sadeq, I. Alani, M. Ahmed, *Opt. Laser Technol.* 2019, **115**, 331.
Crossref | CAS | Web of Science® | Google Scholar

248 Y. Song, K. You, Y. Chen, J. Zhao, X. Jiang, Y. Ge, Y. Wang, J. Zheng, C. Xing, H. Zhang, *Nanoscale* 2019, **11**, 12595.
Crossref | CAS | PubMed | Web of Science® | Google Scholar

249 R. R. Gattass, E. Mazur, *Nat. Photonics* 2008, **2**, 219.
Crossref | CAS | Web of Science® | Google Scholar

250 L. M. Shanyfelt, P. L. Dickrell, H. F. Edelhauser, D. W. Hahn, *Lasers Surg. Med.* 2008, **40**, 483.
Wiley Online Library | PubMed | Web of Science® | Google Scholar

251 E. Fazio, B. Gökce, A. De Giacomo, M. Meneghetti, G. Compagnini, M. Tommasini, F. Waag, A. Lucotti, C. G. Zanchi, P. M. Ossi, et al., *Nanomaterials* 2020, **10**, 2317.
Crossref | CAS | Web of Science® | Google Scholar

252 V. Piotto, L. Litti, M. Meneghetti, *J. Phys. Chem. C* 2020, **124**, 4820.
Crossref | CAS | Web of Science® | Google Scholar

253 R. Jin, Y. C. Cao, E. Hao, G. S. Métraux, G. C. Schatz, C. A. Mirkin, *Nature* 2003, **425**, 487.
Crossref | CAS | PubMed | Web of Science® | Google Scholar

254 M. Condorelli, V. Scardaci, L. D'Urso, O. Puglisi, E. Fazio, G. Compagnini, *Appl. Surf. Sci.* 2019, **475**, 633.
Crossref | CAS | Web of Science® | Google Scholar

255 V. Scardaci, M. Pulvirenti, M. Condorelli, G. Compagnini, *J. Mater. Chem. C* 2020, **8**, 9734.
Crossref | CAS | Web of Science® | Google Scholar

256 Z. Vaseghi, A. Nematollahzadeh, O. Tavakoli, *Rev. Chem. Eng.* 2018, **34**, 529.
Crossref | Web of Science® | Google Scholar

Loading [MathJax]/jax/output/HTML-CSS/fonts/STIX-Web/Normal/Italic/Main.js

257 H. H. Richardson, M. T. Carlson, P. J. Tandler, P. Hernandez, A. O. Govorov, *Nano Lett.* 2009, **9**, 1139.
Crossref | CAS | PubMed | Web of Science® | Google Scholar

258 F. Gu, C. Li, D. Han, Z. Wang, *ACS Appl. Mater. Interfaces* 2018, **10**, 933.
Crossref | CAS | PubMed | Web of Science® | Google Scholar

259 G. Wang, Y. Ling, Y. Li, *Nanoscale* 2012, **4**, 6682.
Crossref | CAS | PubMed | Web of Science® | Google Scholar

260 X. Chen, L. Liu, Z. Liu, M. A. Marcus, W.-C. Wang, N. A. Oyler, M. E. Grass, B. Mao, P.-A. Glans, Y. Y. Peter, et al., *Sci. Rep.* 2013, **3**, 1510.
Crossref | CAS | PubMed | Web of Science® | Google Scholar

261 L. Dong, H. Chu, X. Wang, Y. Li, S. Zhao, D. Li, *Nanophotonics* 2021, **10**, 1541.
Crossref | Web of Science® | Google Scholar

262 F. Quinlan, G. Ycas, S. Osterman, S. A. Diddams, *Rev. Sci. Instrum.* 2010, **81**, 063105.
Crossref | CAS | PubMed | Web of Science® | Google Scholar

263 J. Lousteau, N. Boetti, A. Chiasera, M. Ferrari, S. Abrate, G. Scarciglia, A. Venturello, D. Milanese, *IEEE Photonics J.* 2012, **4**, 194.
Crossref | Web of Science® | Google Scholar

264 S. Masuda, Y. Yanase, E. Usukura, S. Ryuzaki, P. Wang, K. Okamoto, T. Kuboki, S. Kidoaki, K. Tamada, *Sci. Rep.* 2017, **7**, 3720.
Crossref | PubMed | Web of Science® | Google Scholar

265 N. I. Cade, G. O. Fruhwirth, T. Ng, D. Richards, *J. Phys. Chem. Lett.* 2013, **4**, 3402.
Crossref | CAS | Web of Science® | Google Scholar

266 J. Koo, K. Jeong, B.-A. Yu, W. Shin, *Opt. Laser Technol.* 2019, **119**, 105579.
Crossref | CAS | Web of Science® | Google Scholar

267 H. Ahmad, C. Lee, M. A. Ismail, Z. Ali, S. Reduan, N. Ruslan, S. W. Harun, *Appl. Optics* 2016, **55**, 4277.
Crossref | CAS | PubMed | Web of Science® | Google Scholar

268 I. Alani, B. A. Ahmad, M. Ahmed, A. Latiff, A. Al-Masoodi, M. Lokman, S. Harun, *Indian J. Phys.* 2019, **93**, 93.

Loading [MathJax]/jax/output/HTML-CSS/fonts/STIX-Web/Normal/Italic/Main.js

269 H. Ahmad, S. A. Reduan, N. Yusoff, *RSC Adv.* 2018, **8**, 25592.
Crossref | CAS | Web of Science® | Google Scholar

270 Z. I. Rizman, N. F. Zulkipli, H. Arof, M. Yasin, S. W. Harun, *Infrared Phys. Technol.* 2020, **109**, 103433.
Crossref | CAS | Web of Science® | Google Scholar

Download PDF

About Wiley Online Library

Privacy Policy
Terms of Use
About Cookies
Manage Cookies
Accessibility
Wiley Research DE&I Statement and Publishing Policies

Help & Support

Contact Us
Training and Support
DMCA & Reporting Piracy

Opportunities

Subscription Agents
Advertisers & Corporate Partners

Connect with Wiley

The Wiley Network
Wiley Press Room

Copyright © 1999-2022 John Wiley & Sons, Inc. All rights reserved

Loading [MathJax]/jax/output/HTML-CSS/fonts/STIX-Web/Normal/Italic/Main.js